energy&fuels

pubs.acs.org/EF
Article

Sooting Tendency of a Series of Kerosene Surrogates and Blends Containing Various Additives Considered as Sustainable Alternative Fuels

Carl Rainville, Romain Lemaire,* Simon Laflamme, Ibrahima Souno, and Patrice Seers

Cite This: *Energy Fuels* 2025, 39, 6991−7011
Read Online

ABSTRACT: The present work aims at analyzing the sooting tendency of 32 additives considered as potential alternative transportation fuels including 4 C_2−C_5 alcohols, 4 C_7−C_{10} esters, 16 C_4−C_7 furans, 6 C_{10} terpenes, and 2 pyrolysis oils (POs), some of which have seldom (if ever) been studied in the literature. The sooting propensity of each additive, following its mixture with a kerosene surrogate, was characterized using the oxygen extended sooting index (OESI), which is based on the measurement of the smoke point (SP), before being converted into unified index (UI) values for modeling purposes. To that end, a benchmarking analysis of the SP measurement approaches commonly used in the literature was first conducted. The SP of a series of reference fuels from the ASTM D1322 standard were measured using different methods to compare their precision, repeatability, and ease of use. This led to identifying the so-called vision-based algorithm-aided procedure as being the best suited. This method was then selected to test the ability of 8 model fuels to emulate the sooting propensity of a commercial Jet-A. Based on the results obtained, an *n*-dodecane/isocetane/mesitylene/*n*-propylbenzene blend was chosen to be mixed with up to 40 vol % of additives. The measured UI showed that each tested fuel, except for one terpene (myrcene), soots less than the kerosene surrogate. Their soot-suppressing effect was found to decrease in the following order: alcohols > esters > furans > terpenes. Measured data, moreover, allowed extending the predictive capability of a group contribution model (GCM) recently developed through the proposal of dedicated submodels integrating 15 sooting propensity factors suitable for predicting the tendency to soot of furans and terpenes. While satisfactorily simulating measured data, the GCM proved to be valuable for identifying the chemical structures influencing soot production. Finally, although POs exhibit low UI, their high water content, among other things, removes them from consideration as attractive additives.

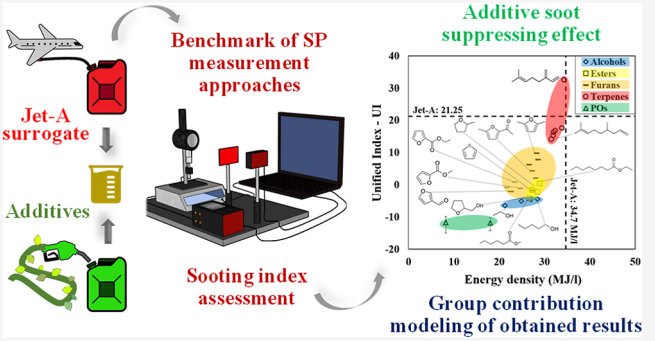

1. INTRODUCTION

Soot particles issued from the incomplete combustion of hydrocarbon fuels adversely affect the climate and human health.[1] Meeting increasingly stringent regulations aimed at restricting particle emissions at the exhaust of practical combustors (comprising engines and turbines), however, requires clarification of the impact of the composition and structure of hydrocarbon fuels on soot formation processes. Although the last half-century has seen major progress in the field,[2−5] more work is still required, especially when it comes to using alternative fuels such as biomass-derived oxygenated substitutes.[6]

Although kerosene is predominantly burnt in aircraft gas turbines, its use in piston engines has also attracted attention due to increasing cases of adulteration of diesel with it and as a response to the single fuel concept (SFC), which promotes the use of a single fuel (JP-8) for aircraft, ground vehicles, and equipment.[7] Alongside the studies focusing on the performance and emissions of compression ignition engines fueled with kerosene and/or kerosene/diesel blends,[7−16] various works have also considered blending kerosene with biodiesels and various oxygenated molecules to fuel this type of engine,[17−22] including diesel power generators,[17,18] as well as spark ignition[23,24] and gas turbine[25] engines. In agreement with the results from ref 8 which showed that adding an oxygen-containing additive such as diethyl ether to diesel/kerosene blends can reduce smoke emissions at the exhaust of a diesel engine, depending on the considered load, numerous engine studies have concluded that mixing kerosene with oxygenates

Received: January 20, 2025
Revised: March 13, 2025
Accepted: March 14, 2025
Published: March 28, 2025

https://doi.org/10.1021/acs.energyfuels.5c00385
Energy Fuels 2025, 39, 6991−7011

Table 1. Composition of a Series of Kerosene Surrogates from the Literature

Surrogate	S1[34] (mol %)	S2[34] (mol %)	S3[35] (wt %)	S4[36] (wt %)	S5[37] (mol %)	S6[38] (mol %)	S7[39] (mol %)	S8[40] (mol %)
n-octane	3.5	3.0						
n-dodecane	40.0	30.0			40.41	28.97	40.11	40.41
n-hexadecane	5.0	12.0						
xylenes	8.5	15.0						
tetralin	8.0	13.0						
decalin	35.0	27.0				31.88	0.5	
n-decane			70	80				
mesitylene			30		7.28			7.28
1,2,4-trimethylbenzene				20				
isocetane						14.24	12.49	29.48
isooctane					29.48		9.8	
toluene						24.91	37.1	
n-propylbenzene					22.83			22.83

such as alcohols (e.g., pentanol in ref 10 and cardanol in ref 22) or esters[20,21] (produced from sunflower and waste cooking oil in refs 20 and 21, respectively) can significantly reduce soot, particulate matter, and smoke emissions. Although the trends ensuing from these studies are noteworthy, they must be supported by theoretical models capable of predicting the sooting behavior of jet fuels, oxygenated additives, and their blends. Much progress has recently been made in developing robust and compact reaction mechanisms to simulate kerosene combustion in diesel engines (see refs 26 and 27 for instance), but more work is needed to properly model the oxidation of kerosene/biofuel blends while clarifying the soot-suppressing effect of the many oxygenated additives in existence, as recalled in the general reviews from refs 6 and 28 as examples. This is particularly critical when considering the increasing number of studies focusing on the analysis of the performance and emissions of internal combustion engines fueled with mixtures composed of kerosene and biofuels, including alcohols[10,22] and esters,[20,21] further noting that there is also growing interest in alternative molecules such as furans[29] or terpenes[30] for their potential use as jet fuel substitutes.

A detailed modeling of the oxidation behavior of kerosene used pure or in blends is impractical due to the complexity of jet fuels, which contain hundreds of compounds. As a workaround, "model fuels" or "surrogates" have commonly been used. These consist of mixtures of relatively small numbers of pure compounds with well-defined and reproducible compositions.[31] Surrogate components are typically chosen to mimic specific physical and/or chemical properties of the target fuel, including its molecular weight, density, boiling point, aromatic content, and/or sooting tendency, mainly depicted through the smoke point (SP), which corresponds to the sooting tendency metric selected by the American Society for Testing and Materials (ASTM) standards for petroleum-derived[32] and synthetic[33] aviation fuels. Among the numerous surrogates proposed in the literature to emulate kerosene, one can refer to the mixtures of *n*-octane, *n*-dodecane, *n*-hexadecane, xylenes, tetralin, and decalin proposed by Eddings et al. in 2005 to reproduce the combustion behavior of JP-8 in pool fires.[34] These model fuels, referred to as "S1" and "S2" in Table 1, were tailored to match the volatility, flash point, sooting tendency, and heat of combustion of JP-8. While the work from Eddings et al.[34] led to the conclusion that formulating an adapted surrogate to mimic the combustion of jet fuels over the lifetime of a batch pool fire was far from straightforward due to the intrinsically transient nature of this type of combustion medium, it still showed that S2 could be considered as a good model fuel to accurately reproduce the burning rate, radiant heat flux, and sooting tendency of JP-8. In the context of experiments performed in laminar and turbulent flames fueled by prevaporized aviation kerosene and binary model fuels comprising normal paraffin and an aromatic, Aksit and Moss concluded that a blend of *n*-decane with 30 wt % mesitylene (S3 in Table 1) could be adapted to satisfactorily reproduce the sooting behavior of typical aviation kerosene as supported by soot volume fraction profiles measured by laser absorption.[35] Later, Honnet et al. demonstrated that a mixture of *n*-decane and 1,2,4-trimethylbenzene (denoted S4 in Table 1) could be considered as a suitable model fuel to capture the critical conditions of extinction and autoignition, as well as the soot volume fractions measured in a laminar nonpremixed flow burning JP-8.[36] In 2012, Dooley et al. proposed a conceptual theory of real fuel oxidation to formulate a surrogate (referred to as S5 in Table 1) comprising *n*-dodecane, isooctane, mesitylene, and *n*-propylbenzene, aimed at emulating the gas-phase combustion kinetic phenomena pertinent to the oxidation of Jet-A.[37] The blend proposed in this comprehensive work coupling experiments performed in a variable-pressure flow reactor, shock tubes, as well as premixed and diffusion flames was demonstrated to exhibit essentially the same global combustion kinetic behavior as that of the target fuel, thus making it an appropriate candidate for the development of combustion kinetic models relevant for gas turbine applications. Kim et al. then developed a surrogate made up of *n*-dodecane, iso-cetane, decalin, and toluene (S6 in Table 1) to mimic the fuel properties affecting the spray development and gas-phase ignition of Jet-A.[38] While this blend properly emulated the Jet-A density and volatility, its use to perform calculations via a detailed chemical mechanism also allowed to predict ignition delay times, in reasonable agreement with the experimental results issued from shock tube and rapid compression machine measurements. More recently, Yu et al. implemented a so-called intelligent approach relying on a mathematical global optimization method to formulate surrogates with physical and gas-phase chemical properties as well as a threshold sooting index (TSI) emulating those of a real jet fuel.[39] In doing so, the authors identified a blend composed of decalin, *n*-dodecane, iso-cetane, isooctane, and toluene (referred to as S7 in Table 1) as being adapted to the development of a skeletal jet fuel surrogate reaction mechanism whose predictions were verified against a series of

https://doi.org/10.1021/acs.energyfuels.5c00385
Energy Fuels 2025, 39, 6991−7011

experimental results in terms of ignition delay times, species concentrations, laminar flame speed, together with spray liquid and vapor penetrations assessed in a constant volume chamber. To conclude, in 2022, Rainville et al.[40] proposed a modified version of the surrogate formulated by ref 37 in which isooctane was replaced by isocetane to better match some properties of a typical Jet-A (molecular weight, density, and volumetric average boiling point) while also leading to a sooting tendency (characterized via a sooting index integrating the SP) closer to the one reported by ref 41. The survey of the literature presented above clearly attests to the continued efforts that have been devoted to the development of surrogates aimed at emulating the combustion behavior of kerosene. The intrinsic validity of the so-formulated model fuels has, however, been assessed based on data acquired under widely varying conditions (pool fire experiments, laminar and/or turbulent flames, shock tube, and rapid compression machine experiments). Furthermore, to the best of the authors' knowledge, no systematic comparison of the sooting propensity of the different surrogates listed in Table 1 has been carried out within the same study. Such a comparison analysis must therefore be undertaken to rule on the relative ability of the surrogate formulations from Table 1 to emulate the sooting propensity of a commercial Jet-A when such fuels are burnt under the same conditions and characterized using the same experimental approach.

Among the metrics commonly used to assess the sooting tendency of hydrocarbon fuels, the smoke point (SP)[42,43] has proven to be a fast and convenient parameter to estimate. It is, moreover, embedded within the formulations of the widely used threshold sooting index (TSI)[44−46] and oxygen extended sooting index (OESI).[47] In short, the SP can be defined as the height of the highest flame produced without smoking when a fuel is burnt in a specific wick-fed test lamp. As for the TSI and OESI, they, respectively, correlate the SP to the fuel molecular weight and to the carbon (n), hydrogen (m), and oxygen (p) atom counts from the generic fuel formula $C_nH_mO_p$. Although the yield sooting index (YSI)[48] and the fuel equivalent sooting index (FESI),[49] which both rely on the measurement of the maximum soot volume fraction in diffusion flames by laser-induced incandescence (LII), enable to precisely estimate the sooting propensity, the SP remains the metric of reference for the rapid screening of the sooting tendency of aviation fuels according to the ASTM standards,[32,33] as noted above. The so-called "manual" SP determination described in refs 32 and 33 is quite user-dependent, however, and hence suffers from possibly significant uncertainties, in addition to low experimental repeatability. To narrow down experimental biases, different approaches for automatically determining the SP have been proposed in a bid to avoid direct flame observation. This notably includes the fuel uptake rate measurement with a threshold imaging (FURTI) method from refs 50 and 51 and the vision-based algorithm-aided procedure from ref 52, hereafter referred to as "VBA". Although highly valuable in reducing experimental errors while leading to better accuracy and repeatability than the ASTM D1322 manual method, selecting a proper approach to measure the smoke point remains far from trivial, thus prompting the need, here again, for further analyses aimed at comparing the relative performance of the manual and advanced methodologies proposed in the literature for the detection of the SP.

In addition to experimentally assessing the sooting tendency of fuels and fuel blends, the implementation of group contribution models (GCMs) can also be highly valuable for better interpreting the trends ensuing from measured data as well as predicting the propensity to soot of a given hydrocarbon based on its composition. This type of simulation tool considers that each component of a fuel can be divided into a set of small groups, also called fragments. A sooting contribution is then assigned to each fragment as a function of its own sooting propensity and of its interaction with its neighbors.[53] The sooting index (SI) of a given molecule i can thus be estimated as a linear sum of the contributions of every group composing it following a relation of type

$$\mathrm{SI}_i = \sum_j N_{ij} \cdot C_j \tag{1}$$

where N_{ij} represents the number of groups of type j composing the compound i, while C_j is the specific contribution of the group j. Using such a group additivity approach, models were notably developed in[47,54,55] to predict the TSI,[54] the OESI,[47] and the YSI[55] of a series of molecules, including oxygenated ones. More recently, Lemaire et al. unified on the same numeric scale the SI values drawn from 15 studies representing more than 700 experimental points to propose a so-called "unified index" (UI).[56] By processing this extensive statistical sample, the authors developed one of the most comprehensive GCMs ever, which integrates sooting propensity factors associated with 93 structural groups composing the main classes of compounds encountered in practical fuels. This model, which was notably used by ref 57, proved to be well suited to predict the sooting tendency of sustainable aviation fuel candidates while leading to results in very good agreement with a quantitative structure−property relationship model developed in ref 57 to predict the TSI of arbitrary mixtures of aliphatic and aromatic hydrocarbons of known composition. The predictive capability of GCMs, is, however, intrinsically dependent on the data set used to train the models. With the exception of the works by refs 55 and 56 who processed data sets embedding a few furans, no GCM truly incorporates detailed submodels for molecules such as furans or terpenes for which contributions are hardly available in the literature. This gap is actually significant when considering the growing attention paid to these compounds, whose properties, and notably their sooting behavior, make them appealing candidates for sustainable transportation biofuels.

In view of the foregoing, the subobjectives of this work, whose main aim is to explore and predict the potential soot-suppressing effects of 32 oxygenated fuels used as kerosene additives and/or substitutes, can be listed as follows

a Comparing 3 different SP measurement approaches, namely, the ASTM D1322 manual method, together with the FURTI and VBA automated procedures, to rule on their respective strengths and weaknesses.

b Comparing the SP and UI of a commercial jet fuel with those of 8 kerosene surrogates (see Table 1) using the measurement approach shown to perform best in a.

c Assessing the soot-suppressing effect of about 30 different oxygenated molecules added to the model fuel identified in b as being the best suited to emulate the sooting tendency of the commercial kerosene tested herein. To this end, the OESI of a series of fuel blends (comprising between 10 and 40 vol % of oxygenated additives) will be measured and converted into UI values. A wide variety of molecules will be tested,

https://doi.org/10.1021/acs.energyfuels.5c00385
Energy Fuels 2025, 39, 6991−7011

Table 2. Main Physicochemical Properties of Jet-A and Model Fuels Considered in This Study

Properties	Jet-A	S1	S2	S3	S4	S5	S6	S7	S8
molecular weight—MW (g/mol)	160.8[63]	151.4[a]/151.5[34]	152.1[a]/152.2[34]	134.8[a]	137.2[a]	138.7[a]	148.6[a]	142.7[a]	171.8[a]
density at 298 K—ρ (kg/m^3)	805[34]	812[b]	819[b]	766[b]	755[b]	760[b]	816[b]	779[b]	788[b]
aromatics—A (vol %)	17.0[65]	11.4	19.4	26.6	17.3	23.0	14.6	21.6	19.3
volumetric average boiling point—VABP (K)	493.4[34]	478.2[c]/484.3[34]	484.0[c]/488.9[34]	444.7[c]	446.4[c]	445.1[c]	471.2[c]	460.6[c]	487.6[c]
freezing point—FP (K)	222.2[65]	254.3[d]	256.4[d]	238.4[d]	240.5[d]	219.5[d]	231.8[d]	224.6[d]	225.2[d]
lower heating value—LHV (MJ/kg)	43.1[65]	43.3[e]	43.1[e]	43.3[e]	43.6[e]/43.6[39]	43.4[e]/43.6[39]	43.1[e]/43.4[39]	43.4[e]/43.4[39]	43.8[e]

[a]Computed using the following relation: $MW = \sum_i x_i \cdot MW_i$, in which x_i and MW_i denote the molar fraction and the molar weight of the i^{th} component of the blend, respectively. [b]Computed using the mixing rule proposed by ref 64, considering the specific volume ν (with $\nu = 1/\rho$), which is a property increasing with more substance according to ref 64, such that $1/\rho = \sum_i w_i \cdot \nu_i$, where w_i and ν_i stand for the mass fraction and the specific volume of the i^{th} component of the blend, respectively. [c]Computed using the relation proposed by ref 66: $VABP = \sum_i \nu_i \cdot BP_i$, where ν_i and BP_i are the volume fraction and the boiling point of the i^{th} component of the blend, respectively. Note that although strictly speaking, the above relation is inadequate to properly define the average boiling point of a mixture, it is still common practice to use it to estimate the properties of petroleum fractions by standard industrial methods as well as for comparison with the values from the literature, as pointed out by ref 67. [d]Computed based on the relation taken from ref 68: $FP = \sum_i \nu_i \cdot FP_i$, where FP_i stands for the freezing point of the i^{th} component of the blend. [e]Computed based on the ASTM D3338 correlation, in which VABP is used as a volatility metric:[69] $LHV = (5528.73 - 92.6499 \cdot A + 10.1601 \cdot VABP + 0.314169 \cdot A \cdot VABP)/\rho + 0.0791707 \cdot A - 0.00944893 \cdot VABP - 0.000292178 \cdot A \cdot VABP + 35.9936$. Note that the values of the properties required to operate the above calculations were taken from the database obtained from the National Institute of Standards and Technology.[70]

including 4 alcohols (ethanol,[14] propanol,[25] butanol,[23,25] and pentanol,[10,25] which are commonly considered to be mixed with kerosene in compression ignition[10,14,25] and spark ignition[23] engines), 4 esters (including methyl hexanoate and ethyl octanoate in addition to butyl butyrate and methyl octanoate which have been identified as promising candidates for blending with aviation kerosene[58,59]), together with 16 furans and 6 terpenes whose potential use as jet fuel substitutes has been recently investigated.[29,30] Of note, the present list of additives is clearly far from covering the full range of sustainable fuel candidates intended for use as kerosene substitutes. Indeed, the present work does not consider aldehydes or ketones, for instance, whose propensity to soot was already investigated in some of our previous works.[49,56] Similarly, organometallic fuel additives[60] fall outside of the scope of the present work while synthetic hydrocarbons derived from power-to-liquid (PtL) processes[61] were not investigated herein since the sooting tendency of their main components is already well documented in the literature.

d Extending the GCM model previously developed in ref 56 by assessing the sooting contributions of various functional groups entering into the composition of furans and terpenes via the processing of the experimental database newly developed in c. Doing so will notably lead to the proposal of dedicated submodels suitable for predicting the propensity to soot of these specific oxygenates for which relatively few data are available.

e Testing the sooting behavior of two pyrolysis oils (POs) produced from spruce wood (SW) and switchgrass (S), which will be added to the surrogate identified in b at vol % up to 40%. Given the number of engine tests conducted in recent years with blends composed of kerosene and bio-oils or cooking oils,[18,20,21] and further considering the interest which has been growing in converting biomass-derived pyrolysis bio-oil to biojet fuel (see ref 62 and references therein), this complementary analysis will thus allow to extend the scope of the present study by providing original data related to the sooting propensity of POs and their blends with a jet fuel surrogate (no such data being reported in the literature, to the best of the authors' knowledge).

To tackle these different points, the present article is structured as follows: Section 2 details the fuels used and the experimental platform. It also introduces and compares the different SP measurement approaches considered in this work (a). For its part, Section 3 is devoted to the presentation of the experimental results obtained regarding the identification of a proper kerosene surrogate (b), followed by an analysis of the sooting behavior of the above-listed oxygenated additives (c). Observed trends are then discussed and modeled by means of the improved group increment model proposed as part of this study (d). Finally, the data collected during tests conducted with blends of kerosene surrogate and pyrolysis oils are detailed (e).

2. MATERIALS AND METHODS

2.1. Fuels. The main thermophysical properties of the 8 surrogates listed in Table 1 are compared with those of a commercial Jet-A (used as a reference fuel in this work) in Table 2. Computed properties are notably compared with those issued from the literature when available. As can be seen by looking at the data presented in Table 2, computed MW and VABP for S1 and S2 match the values reported in ref 34. Similarly, the mean relative deviation between the LHV estimated herein and those reported in ref 39 is less than 3%. Although the potential uncertainties surrounding the assessment of the values reported in Table 2 are not of major concern in the context of the present work, whose main focus is on the sooting propensity, as explained in Section 1, the observations presented above still tend to exemplify the overall consistency of the physicochemical properties we estimated. One can thus note that S1 is the model fuel that best emulates the density of kerosene. Table 2, moreover, shows that S2 is best suited to properly reproduce the molecular weight and the lower heating value of Jet-A, although it leads to the highest freezing point discrepancy. This latter property is best mimicked by S7, while the aromatic content and the VABP are best emulated by S4 and S2/S8, respectively. By averaging the relative deviations computed when comparing the different properties of Jet-A with those of each model fuel, one can finally note that S3 is the surrogate leading to the highest overall discrepancy (~16.6%), notably due to its high aromatic

https://doi.org/10.1021/acs.energyfuels.5c00385
Energy Fuels 2025, 39, 6991−7011

content, while S8 conversely leads to the best agreement (~5.2% with relative deviations comprised between 1.2% for VABP and 13.5% for A).

In addition to the fuels listed in Table 2, 30 pure additives (all oxygenated, with the exception of myrcene) were selected to be blended with the kerosene surrogate identified in Section 3.1 as being the most adapted to emulate the sooting propensity of Jet-A. The tested molecules include 4 alcohols, 4 esters, 16 furans, and 6 terpenes, as detailed in Table 3. Furthermore, two pyrolysis oils (POs) were also considered for use as additives. These were produced from the pyrolysis of spruce wood (SW) and switchgrass (S) samples whose detailed compositions can be found in ref 71. Both feedstocks were thermally treated in an Auger reactor (described in detail in refs 72 and 73 among others), which is located at the Deschambault research center of the Research and Development Institute for the Agri-Environment in Quebec (Canada). Produced POs were obtained by processing SW and S at temperatures of 516 and 525 °C, with reaction times of 80 and 120 s, respectively.[72] Their main physicochemical properties are summarized in Table 4. As for their chemical composition, the oil phase of the SW PO was shown in ref 73 to contain 6.2% carboxylic acids, 10.5% nonaromatic aldehydes, 12.2% nonaromatic ketones, 3.4% benzenediols, 14.6% carbohydrates, 12.5% furans, 1.7% phenols, and 26.9% guaiacols (expressed in % of relative content as determined by gas chromatography−mass spectrometry). Regarding the S PO, the authors in ref 74 found that it was typically composed of 36.2% alkanes, 20.5% phenols, 14.1% aromatics, 4.2% furans, 5.1% ketones, 8.7% fatty methyl esters and acids, 7.4% alcohols, 2.4% esters, and 1.5% amides.

Of note, the analysis of the sooting propensity of fuel blends containing various amounts of POs requires implementing an emulsification procedure, as is done in refs 80−82 as examples. To identify the adapted proportions of surfactant and cosurfactant leading to homogeneous and stable blends, a full design of experiments (not detailed herein for brevity) was built, considering 3 different emulsifiers (Span 80, Tween 80, and Atlox 4914), together with 1 cosurfactant (methanol), whose proportions were varied to obtain bio-oil-to-emulsifier weight ratios of between 1.0 and 4.0 and cosurfactant-to-emulsifier weight ratios (C/E ratio) of between 0.5 and 1.0. Methanol was specially selected since short-chain alcohols are known to induce stronger hydrogen bonding while having a higher polarity and hydrophilic−lipophilic balance (HLB). They hence exhibit a better solubility in polar fluids, making methanol a cosurfactant that mixes very well into bio-oils.[81] Based on the experimental procedures described in refs 81 and 82, the solutions, composed of the emulsifier, the cosurfactant, and the model fuel, were first homogenized for 3 min. Thereafter, the POs were added into the obtained blends and mixed for 6 min with an emulsifying temperature set to 40 °C, as in ref 82. Considering that the higher the bio-oil content, the lower the critical C/E ratio for successful emulsification, and further noting that the addition of alcohol as the cosurfactant significantly improves the stability of the mixtures (especially for blends with high PO content),[81] the emulsification tests were preliminarily performed with mixtures containing the highest weight percentage of PO considered in this work (i.e., 43.52 wt % which corresponds to a blend containing 40 vol % of oil in the case of the SW PO). Once the emulsions were prepared, the phase separation was checked every 20 min for the first 6 h, every 6 h for the following 48 h, and every 24 h for the remainder of the stability tests, which lasted 30 days. The obtained results showed that Atlox 4914 performed better than Span 80 and Tween 80, which agrees with the conclusions from ref 80. This trend can notably be traced to the fact that Atlox 4914 (whose HLB value is 6) combines the hydrophilic portion of polyethylene glycol and the hydrophobic portion of poly alkyd resin according to ref 80. Blends containing 7.5 wt % of Atlox 4914 and 5.0 wt % of methanol, moreover, demonstrated high stability, as exemplified by the absence of phase separation for a period of at least 30 days. Since this duration is much greater than the time separating the preparation of the samples and the SP measurements, the above formulation was thus considered satisfactory for the purposes of the present work. It is, however, not claimed here that the latter should be considered as valid for other uses such as engine tests and/or commercial applications. Further characterizations, including long-term stability assessment among others, would indeed be required to that end, although clearly falling out of the scope of this study.

Finally, and for the comparison analysis of the relative performance of the different SP measurement approaches (see Section 2.3), the 7 reference fuels from the ASTM D1322 standard were considered.

Table 3. List of Pure Molecules Considered as Additives in the Present Work

Name	Abbreviation	Formula	Structure
1-ethanol	ET	C_2H_6O	
1-propanol	PR	C_3H_8O	
1-butanol	BU	$C_4H_{10}O$	
1-pentanol	PE	$C_5H_{12}O$	
methyl hexanoate	MH	$C_7H_{14}O_2$	
butyl butyrate	BB	$C_8H_{16}O_2$	
methyl octanoate	MO	$C_9H_{18}O_2$	
ethyl octanoate	EO	$C_{10}H_{20}O_2$	
Furan	FUR	C_4H_4O	
2,3-dihydrofuran	23DHF	C_4H_6O	
2,5-dihydrofuran	25DHF	C_4H_6O	
tetrahydrofuran	THF	C_4H_8O	
Furfural	2FF	$C_5H_4O_2$	
3-furaldehyde	3F	$C_5H_4O_2$	
2-methylfuran	2MF	C_5H_6O	
furfuryl alcohol	2HMF	$C_5H_6O_2$	
2-methyltetrahydrofuran	MTHF	$C_5H_{10}O$	
tetrahydrofurfuryl alcohol	HMTHF	$C_5H_{10}O_2$	
2,5-dimethylfuran	25DMF	C_6H_8O	
2-ethylfuran	2EF	C_6H_8O	
methyl-2-furoate	M2F	$C_6H_6O_3$	
2-acetyl-5-methylfuran	2A5M	$C_7H_8O_2$	
ethyl-2-furoate	E2F	$C_7H_8O_3$	
ethyl-3-furoate	E3F	$C_7H_8O_3$	
myrcene	MC	$C_{10}H_{16}$	
geranial	GNA	$C_{10}H_{16}O$	
geraniol	GNO	$C_{10}H_{18}O$	
citronellal	CTL	$C_{10}H_{18}O$	
linalool	LNL	$C_{10}H_{18}O$	
1,8-cineole	18CL	$C_{10}H_{18}O$	

https://doi.org/10.1021/acs.energyfuels.5c00385
Energy Fuels 2025, 39, 6991−7011

Table 4. Properties of Spruce Wood (SW) and Switchgrass (S) Pyrolysis Oils (POs)

PO	SW	S
Elemental Analysis (wt %)		
C	41.61	22.23
H	6.65	8.25
N	0.03	0.10
S	0.00	0.00
O[a]	51.72	69.41
Supplementary Physicochemical Properties		
water content (wt %)	22.74	29.05
pH	1.982	2.786
density (g/cm^3)	1.23	1.12
MW (g/mol)	351[b]	284[c]
higher heating value—HHV (MJ/kg)[d]	17.12	10.03

[a]By difference. [b]Mean of the values reported in refs 75−77 for PO produced from woody biomass. [c]Taken from ref 78. [d]Computed based on the relation proposed by ref 79: HHV = 0.363302·C + 1.087033·H − 0.100992·O, in which C, H, and O denote the weight percentages of carbon, hydrogen, and oxygen, respectively, which are issued from the elemental analysis of the POs.

They consist of blends of toluene and isooctane with vol % of the latter of 60, 75, 80, 85, 90, 95, and 100%.[32]

2.2. Experimental Setup. The experimental arrangements typically used to measure the SP through the manual, FURTI, and VBA approaches were extensively described in refs 32, 51, and 52, respectively. Only a short description of these setups will therefore be given below. The focus herein will indeed be more on the main features of the components selected to build the platform used in this work, which is depicted in Figure 1.

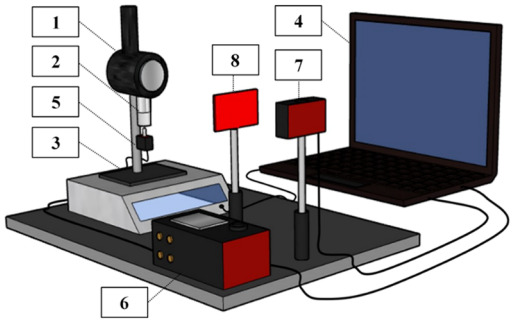

Figure 1. Diagram of the SP test experimental setup: (1) ASTM D1322 SP wick-fed lamp; (2) candle; (3) analytical balance; (4) computer; (5) piezo inertia actuator; (6) controller; (7) CMOS camera; (8) long-pass filter. Note that the balance and the long-pass filter are used solely when implementing the FURTI method, while the actuator and its controller are required only when measuring the SP by means of the VBA approach.

The ASTM D1322 standardized test diffusive lamp (denoted as 1 in Figure 1) is the main component of each SP measurement setup. It comprises (from bottom to top) a candle (referred to as 2 in Figure 1) with its socket, a gallery, a wick guide, a scale positioned behind the flame inside the lamp body, and a chimney (see ref 32 for more details regarding the main components of a standard SP lamp). For the implementation of the FURTI method, the wick-fed lamp was placed on a Sartorius BCE6202-1S analytical balance (denoted 3 in Figure 1) having a capacity of 6200 g and a precision of 10 mg, as in ref 51. This balance was interfaced with a computer (denoted as 4 in Figure 1) by means of a software application provided by the manufacturer to continuously save weight readings with a view to computing the fuel uptake rates for each measuring point (see Section 2.3.2). As for the setup used to measure the SP with the VBA approach, it includes a Thorlabs PIA25 Piezo Inertia Actuator and a Thorlabs KIM101 K-Cube controller (connected to the computer), respectively, referred to as 5 and 6 in Figure 1. Using a specifically devoted Thorlabs software application, the flame height can be increased by moving the tank nut of the lamp at a fixed rate set to 350 steps/s in this work. For both the FURTI and VBA automated procedures, the flame images were captured using a Thorlabs CS165CU1 Zelux camera (denoted 7 in Figure 1) having a resolution of 1440 × 1080 pixels. The frame rate was set to 25 frames per second (fps), which is higher than both the 1 and 20 fps reported in refs 51 and 52, respectively. Furthermore, the optical equipment was arranged so as to obtain a maximum millimeter per pixel resolution of 0.05 mm/pixel, which is better than the 0.0745 mm/pixel from ref 51 and equal to the resolution obtained by ref 52. Note also that a long-pass filter identical to the one used in ref 51 (denoted 8 in Figure 1) was placed in front of the camera when measuring the SP by means of the FURTI method to faithfully reproduce the procedure described in ref 51. The flame images were then saved by the computer connected to the camera before being processed using in-house-developed algorithms written in MATLAB.

2.3. SP Measurement Approaches. *2.3.1. SP Measurements by Means of the Manual ASTM D1322 Approach.* To compare the relative performance of manual and automated SP measurement approaches, the procedure described in ref 32 was first applied to measure the SP of the 7 reference fuels from the ASTM D1322 standard (see Section 2.1). To that end, the tank of the wick-fed lamp was first filled with the fuel, whose sooting propensity needed to be characterized. The wick was then lit before the fuel tank nut was manually rotated to increase the flame height in an attempt to measure, thanks to the scale positioned behind the flame, the height for which the latter started to smoke. The tests were performed while strictly following the procedure described in ref 32 regarding the calibration, warm-up, and handling of the wick-fed lamp and cotton wicks during and after the measurements. The results obtained are presented in Table 5, which compares the SP we measured with the standard values reported in ref 32. Note that the focus is solely on the measurements taken when using the manual method at this stage, while the results issued from the implementation of the FURTI and VBA methods are discussed more specifically in Sections 2.3.2 and 2.3.3.

As can be seen by looking at the results reported in the fifth column of Table 5, the mean experimental bias related to the SP measurements performed with all the calibration fuels is of the order of ± 2.1 mm, which is globally in line with the ± 2.6 mm reported in ref 51. Regarding the relative differences between standard and measured SP values (see the eighth column of Table 5), they range between 3.27 and 12.93%, with a mean of 8.43%, which, here again, is consistent with the ∼10% found in ref 51.

2.3.2. SP Measurements by Means of the FURTI Method. The experimental procedure allowing to determine of the SP by means of the FURTI approach is described in detail in ref 51 to which the reader is referred for more information. In short, the method consists in capturing the transition from a nonsooting flame with a well-defined round flame tip to a sooting one, with a sharp flame tip. To this end, the flame evolution is recorded by a camera while the fuel uptake rate is simultaneously determined for different flame heights by means of the balance on which the SP lamp is placed (see Section 2.2). By plotting the evolution of the flame height (H_f) as a function of the fuel uptake rate (FUR), one can then assess the SP, which corresponds to the first inflection point displayed on the obtained graph.

As in the work by Graziano et al.,[51] the FUR was measured for 17 to 40 different H_f during each test. Measurement points had a fixed duration of 120 s, and flame images were recorded at a frame rate of 25 fps (thus leading to 3000 images captured per measurement point). The images were then postprocessed using an intensity gradient approach to determine the flame contour with a view to inferring averaged H_f values for each measurement point. To that end, we implemented an in-house algorithm written in MATLAB, similar to the one described in ref 51 whose use allowed to detect of the

https://doi.org/10.1021/acs.energyfuels.5c00385
Energy Fuels 2025, 39, 6991−7011

Table 5. SP Measurement Results[a]

fuel #	isooctane (vol %)	toluene (vol %)	standard SP[32] (mm)	SP manual (mm)	SP FURTI (mm)	SP VBA (mm)	RD manual (%)	RD FURTI (%)	RD VBA (%)
1	60	40	14.7	16.6 ± 1.90	14.34 ± 0.36	14.97 ± 0.27	12.93	2.45	1.84
2	75	25	20.2	19.1 ± 1.10	19.45 ± 0.75	20.65 ± 0.45	5.45	3.71	2.23
3	80	20	22.7	20.2 ± 2.50	22.04 ± 0.66	22.37 ± 0.33	11.01	2.91	1.45
4	85	15	25.8	23.5 ± 2.30	24.93 ± 0.87	26.14 ± 0.34	8.91	3.37	1.32
5	90	10	30.2	27.4 ± 2.80	29.23 ± 0.97	30.87 ± 0.67	9.27	3.21	2.22
6	95	5	35.4	38.3 ± 2.90	34.39 ± 1.01	36.11 ± 0.71	8.19	2.85	2.01
7	100	0	42.8	41.4 ± 1.40	42.21 ± 0.59	42.46 ± 0.34	3.27	1.38	0.79

[a]Note that the smoke points measured in the present work are systematically derived from the averaging of 3 tests, as done in ref 52. Note also that RD stands for relative difference in the eighth, ninth, and tenth columns of the table.

flame tip edge based on gradient (Figure 2a) and raw intensity (Figure 2b) images. Once the flame height (i.e., the highest position

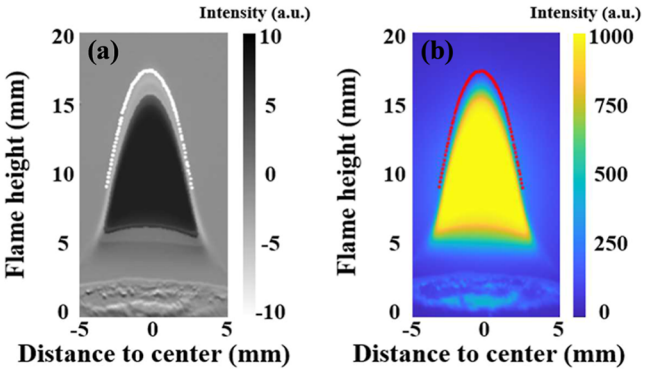

Figure 2. Grayscale gradient (a) and raw (b) images of an isooctane flame (flame edge indicated with white and red dashed lines in (a) and (b), respectively).

of the detected contour) is estimated, one can plot a H_f over the FUR graph, as depicted in Figure 3. The SP, which is marked by full red

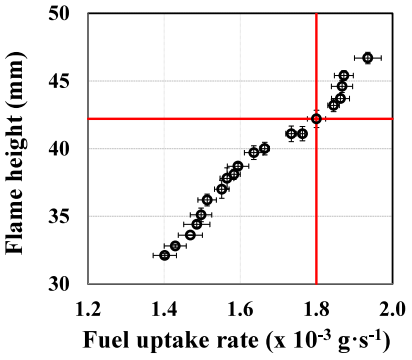

Figure 3. Flame height over fuel uptake rate for isooctane.

lines in this figure, can thus be inferred, noting that the error bars drawn there depict the absolute H_f and FUR errors computed following the calculation procedure extensively described in ref 51 to which the reader is referred for more details.

Before conducting systematic measurements with the FURTI method using the calibration fuels listed in Table 5, repeatability tests were carried out based on the procedure adopted by ref 52. To that end, fuels #3 and #7 were selected and their SP were measured by performing 10 consecutive tests, as in ref 52. The obtained results, which are presented in Figure 4 for fuel #7 (i.e., isooctane) as an example, show that the measured smoke points (depicted by black circles) are all comprised between the lower and upper limits (represented by full black lines) computed based on the repeatability

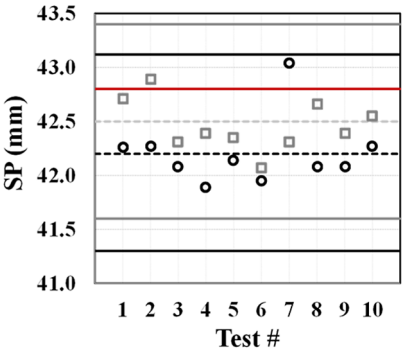

Figure 4. Repeatability test regarding the assessment of the SP of isooctane (fuel #7) when using the FURTI (black circles) and VBA (gray squares) methods. Note that the mean SP (depicted by dashed black and gray lines for the FURTI and VBA methods, respectively) is compared with the reference value taken from the ASTM D1322[32] (represented through a full red line). Black (FURTI) and gray (VBA) full lines finally represent the lower and upper limits between which SP values must be comprised to fulfill the ASTM D1322 repeatability criterion.

criterion set in ref 32. Note that similar results (not reported for brevity) were also obtained with fuel #3. One can conclude that the repeatability associated with the FURTI approach is satisfactory.

To conclude, it is noteworthy that the mean SP estimated for isooctane with the FURTI approach (see the dashed black line in Figure 4) is relatively close to the standard value reported in ref 32 (see the full red line in Figure 4). A relative difference of 1.38% can indeed be computed, as detailed in Table 5. Furthermore, the mean experimental bias is just ±0.74 mm (compared to the ±2.1 mm obtained with the manual method) and the mean relative difference between the standard and measured SP is 2.84%, which is significantly lower than the 8.43% estimated in Section 2.3.1. In line with the conclusions from ref 51, the FURTI method thus proved to significantly reduce the experimental bias in the SP height in comparison with the standard manual method from the ASTM D1322.

2.3.3. SP Measurements by Means of the VBA Method. The vision-based algorithm method from ref 52 consists in continuously acquiring flame images while automatically increasing the flame height at a fixed rate using an actuator attached to the lamp nut (see Section 2.2) until the SP is reached. Each image is then postprocessed by being converted to a grayscale format, while a threshold binarization technique coupled with basic filter operations is applied to assess the flame shape and define specific regions that will subsequently be used to estimate the SP. To that end, we implemented an in-house algorithm written in MATLAB, similar to the one used in ref 52. Images collected were first converted to a grayscale format, with each pixel having a luminous intensity value ranging from 0 (pure black) to 255 (pure white), as illustrated in Figure 5a. Two thresholds whose values were set to 90 (35% of 255) and 230 (90% of 255) were then used to determine the group of pixels corresponding to the flame

https://doi.org/10.1021/acs.energyfuels.5c00385
Energy Fuels 2025, 39, 6991−7011

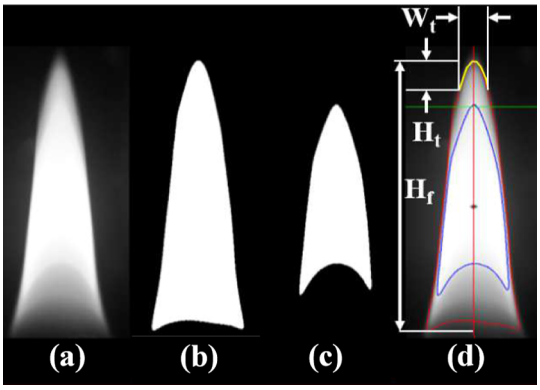

Figure 5. Flame image postprocessing steps: (a) flame image converted to grayscale, (b) flame shape threshold, (c) flame core threshold, and (d) assessment of the flame-specific dimensions.

shape and flame core (see Figure 5b and c, respectively), with the other pixels being given a value of 0. Finally, three specific flame dimensions were calculated (see Figure 5d), namely, the flame tip width (W_t), the flame tip height (H_t), and the flame height (H_f). Based on several experimental tests,[52] it was found that the flame tip can be obtained from the top flame edge, centered in the middle point of the core, with a length of 40% of the width of the bottom flame edge. By measuring the H_t and W_t values, one can finally estimate the tip ratio R_t defined as per eq 2

$$R_t = \frac{H_t}{W_t} \tag{2}$$

By plotting the evolution of R_t as a function of the flame height H_f, one obtains a two-part graph (see Figure 6) in which the point separating the two first-order curves fitted to the points showing linearity (see the blue lines in Figure 6) corresponds to the SP.

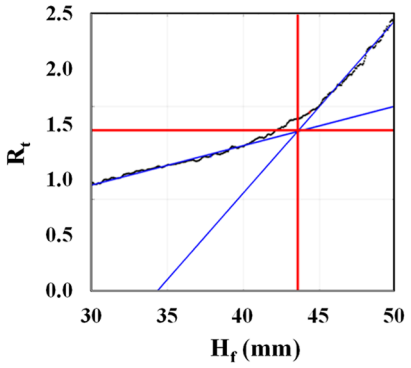

Figure 6. Example of $R_t = f(H_f)$ graph obtained in the case of isooctane.

As can be seen by looking at the gray squares and the dashed gray line plotted in Figure 4, which are well comprised between the two full gray lines, the VBA approach also meets the repeatability criterion set in ref 32. Furthermore, the results reported in Table 5 show that a mean experimental bias and a relative difference of ±0.44 mm and 1.69% are obtained, which is in good agreement with the results reported in ref 52 (±~0.6 mm and 2.6%) while being lower than the values assessed with the manual and FURTI approaches.

2.3.4. Discussion Regarding the Relative Strengths and Weaknesses of the Different SP Measurement Approaches Tested Herein. The results reported in Sections 2.3.1, 2.3.2, and 2.3.3 demonstrated that both the FURTI and VBA automated SP measurement approaches are more precise and accurate than the conventional manual procedure from ref 32. Although the mean experimental biases and relative differences computed with the FURTI and VBA methods are quite similar, the VBA approach was still found to perform slightly better. In view of the foregoing, the VBA method was, therefore, selected to operate the measurements detailed in Section 3. Indeed, despite a relatively simple implementation, the manual method from the ASTM D1322 standard is heavily user-dependent and is likely to involve errors due to the inherent uncertainty of visual flame observation, as evidenced by the results reported in Section 2.3.1. As for the VBA approach, it has been found to be more straightforward to implement than the FURTI technique while being less open to interpretation. Indeed, finding the intersection of the two linear sections depicted on the curves indicating the evolution of the tip ratio over the flame height (see Figure 6) leaves less room for the operator to assess the SP than when attempting to identify the first inflection point displayed on the plot of the flame height as a function of the fuel uptake rate (see Figure 3). Furthermore, the H_f over FUR curve used in the FURTI method may suggest multiple inflection points requiring the operator to select the point associated with the onset of smoke production observed during the test. Finally, the global test duration is much longer with the FURTI method than with the VBA one. As an example, estimating the SP of the reference fuel #7 was done in under 7 min when setting the operating parameters of the VBA procedure as described in Section 2.2 versus 34 min when implementing the FURTI approach, even when taking only 17 measurement points, which is the minimum used in ref 51. One should, however, note that it is not claimed here that one SP measurement approach should be preferred over another. Rather, this discussion mainly aims to identify the potential strengths and weaknesses of the tested methods as a function of the application targeted by this paper, which is what led us to select the VBA method for the reasons described above. The latter approach should thus not be considered as being the best suited for the SP assessment since complementary tests, including interlaboratory comparisons as well as statistical error propagation analyses, for instance, would be a must if definitive information regarding which technique performs the best is to be derived.

2.4. Converting Measured SP into SI Values. The OESI was selected as an indicator to characterize the sooting tendency of the kerosene surrogates and of the blends comprising alcohols, esters, furans, terpenes, and pyrolysis oils as additives. Among the reasons for this choice was the fact that the formulation of the OESI integrates the SP, which is, as stated in Section 1, the metric of reference for assessing the sooting propensity of aviation fuels according to ASTM standards.[32,33] It, moreover, correlates the SP to the carbon (n), hydrogen (m), and oxygen (p) atom counts from the generic fuel formula $C_nH_mO_p$, as per eq 3. Consequently, while being quite equivalent to the TSI for nonoxygenated molecules,[47] the OESI remains well adapted for the characterization of oxygenated molecules, making it perfectly adapted for the purposes of this research.

$$\mathrm{OESI} = a' \cdot \left(\frac{n + m/4 - p/2}{\mathrm{SP}} \right) + b' \tag{3}$$

Of note, the apparatus-dependent constants a' and b' integrated in eq 3 have been adjusted following the procedure described in ref 56 to obtain OESI values matching those reported by Barrientos et al.[47] when analyzing a series of oxygenated and nonoxygenated molecules (see ref 56 for more details). Note also that we implemented the group contribution model (GCM) previously proposed in ref 56 (see Section 2.5) to allow a more in-depth interpretation of the results reported in Section 3. As explained in ref 56, this GCM was developed by processing a comprehensive set of TSI, OESI, YSI, and FESI values obtained from 15 studies, which were converted into a unified index (UI) in order to fit the same numeric scale. Proceeding as such allowed us to create and analyze one of the most extensive sets of SI values ever, noting that the greater the amount of data available, the greater the degree of confidence related to the statistical analysis performed to derive sooting contribution factors, and the more robust the GCM. Consequently, measured OESI were ultimately converted into UI using the correlation provided in Figure 1 of ref 56 in order to

https://doi.org/10.1021/acs.energyfuels.5c00385
Energy Fuels 2025, 39, 6991−7011

allow conducting the modeling work presented in Section 3. Incidentally, the selection of the UI as a sooting index is ultimately all the more relevant and useful as this indicator can be easily converted into the OESI, YSI, FESI, as well as TSI for nonoxygenated hydrocarbons, using the correlations proposed in ref 56. The results detailed in the present work will therefore be easily usable for comparison with the trends issued from other works carried out using other conventional sooting metrics.

2.5. Group Contribution Model. The implemented GCM is extensively described in ref 56. In short, it is based on the approach developed by Cohen and Benson[83,84] to infer the thermochemical and physical properties of organic compounds. It consists of decomposing any molecule into sets of standard functional groups or fragments to which a specific contribution to the property of interest (i.e., the propensity to soot, in this case) is assigned. The Cohen and Benson theory considers nearest−neighbor interactions to estimate contribution factors which allow accounting for different possible soot formation pathways. Each group is defined as a combination of a polyvalent atom linked to ligands specified between brackets after a dash. Following the nomenclature proposed in ref 83, the carbonyl group is treated as a polyvalent unit. Furthermore, a distinction is made between C atoms depending on the structure in which they are involved. Carbons in functional groups presenting double and triple bonds or aromatic and fused cycles are indeed typically denoted C_d, C_t, C_B, and C_{BF}, respectively, while C atoms involved in furanic cycles are identified as C_F, following ref 85. Considering the so-called unified index as a sooting propensity indicator (see Section 2.4), one can calculate the UI of any compound i using eq 1 while substituting SI_i with UI_i therein. Based on the 93 C_j values reported in ref 56, one can estimate the UI of most of the hydrocarbons encountered in practical fuels. Furthermore, the UI of fuel blends can be calculated by means of an additivity rule of the type

$$UI_{mixture} = \sum_i X_i \cdot UI_i \quad (4)$$

where X_i and UI_i denote the mole fraction and the UI of the i^{th} component of the blend, respectively. Since the present work focuses particularly on furans and terpenes, which were almost absent from the database processed to build the GCM from ref 56, the contributions (C_j) of different fragments composing these types of molecules were unknown. We therefore estimated these contributions (whose values will be detailed in Section 3) by means of an optimization procedure which aims at minimizing an objective function defined as a least-squares sum between UI derived from measured OESI and theoretical values computed using eqs 1 and 4. To that end, we used a genetic algorithm-based optimization routine identical to the one recently used in refs 86 and 87 to parameterize laser-induced incandescence models and in ref 88 to derive devolatilization kinetic parameters. In doing so, the predictive capability of the group contribution model developed in ref 56 was thus extended through the inclusion of contribution factors for structural fragments enabling the prediction of the sooting propensity of furans and terpenes, in addition to the different classes of molecules already integrated within the original version of the model.

3. RESULTS AND DISCUSSION

3.1. Identification of a Suitable Surrogate to Mimic the Sooting Propensity of Jet-A. Table 6 compares the sooting propensity of the 8 surrogates listed in Table 1 with that of Jet-A. Note that the SP of the latter was measured using the same commercial fuel as that previously used in ref 89. Its approximate chemical formula (i.e., $C_{11.6}H_{21.7}$) is in line with the elemental compositions reported in the literature for JP-8 and Jet-A, whose formulas typically range from $C_{10.9}H_{20.9}$ to $C_{12.0}H_{23.0}$, according to ref 31. It is, moreover, also consistent with the molecular formula reported by ref 41 for Jet-A (i.e., $C_{11.4}H_{22.1}$), whose SP and corresponding UI are reported in Table 6 for comparison. Furthermore, and to better illustrate

Table 6. Sooting Tendency of Jet-A and Its Surrogates

fuel	molecular formula	SP (mm)	UI[a]	RD[b] (%)
Jet-A	$C_{11.4}H_{22.1}$ [41]	22.0[41]	22.10	
	$C_{11.6}H_{21.5}$	22.8 ± 0.29	21.25 ± 0.33	
S1	$C_{10.86}H_{20.84}$	28.1 ± 0.34	15.31 ± 0.23	27.95
S2	$C_{10.96}H_{20.34}$	24.8 ± 0.28	17.89 ± 0.25	15.81
S3	$C_{9.66}H_{18.63}$	21.6 ± 0.28	18.44 ± 0.30	13.22
S4	$C_{9.77}H_{19.72}$	32.9 ± 0.36	11.00 ± 0.17	48.24
S5	$C_{9.92}H_{19.43}$	25.5 ± 0.39	15.56 ± 0.31	26.78
S6	$C_{10.69}H_{20.11}$	24.8 ± 0.19	17.43 ± 0.16	17.98
S7	$C_{10.24}H_{19.50}$	25.4 ± 0.21	16.10 ± 0.15	24.24
S8	$C_{12.28}H_{24.14}$	24.1 ± 0.24	21.77 ± 0.23	2.45

[a]Computed by converting the OESI values (see eq 3) which integrate the SP reported in this table by means of the correlation provided in Figure 1 of ref 56. [b]Computed while considering the UI of the Jet-A analyzed in the present work as a reference.

how the propensity to soot of each tested surrogate compares with the most plausible range of UI corresponding to kerosene, the results obtained are plotted in Figure 7, where the red

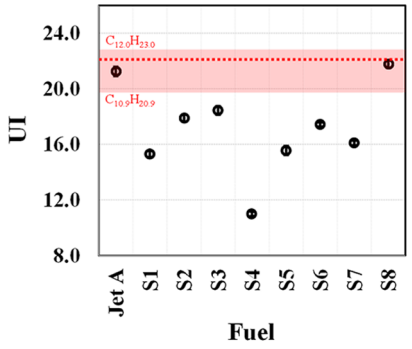

Figure 7. UI estimated in the present work based on the SP measured with Jet-A and surrogates S1 to S8. The red region on the graph delimits the UI values computed while considering a mean SP of 22.7 and approximate chemical formulas ranging from $C_{10.9}H_{20.9}$ to $C_{12.0}H_{23.0}$. The red dotted line corresponds to the UI calculated based on the SP and chemical formula reported by ref 41. Note also that the error bars plotted on the graph were computed based on the experimental bias assessed during the SP measurements.

region delimits the upper and lower UI computed for Jet-A, taking an SP of 22.7 (mean of the value obtained herein (22.8 mm) and of the SP reported in ref 34 (24.5 mm), ref 37 (22.1 mm), ref 41 (22.0 mm), ref 90 (24 mm), and ref 91 (21.0 mm)) while considering the approximate chemical formulas reported by ref 31 (i.e., $C_{10.9}H_{20.9}$ and $C_{12.0}H_{23.0}$). One can then clearly see that S8 is the model fuel that best emulates the sooting propensity of the tested kerosene, with a UI difference of 2.45% (see Table 6). While being consistent with the fact that the composition of S8 was adjusted in ref 40 to better mimic the sooting propensity of Jet-A (see Section 1), it is noteworthy that the UI of this surrogate also matches very well the value computed based on the data reported in ref 41 (see the red dotted line in Figure 7). On the other hand, and as can be seen by looking at the results reported in Table 6 and Figure 7, the use of S2 and S3 leads to sooting index values relatively close to that of Jet-A (with relative differences (RD) of 15.81 and 13.22%, respectively), although the UI of both of these model fuels, similarly to those of the other tested surrogates, fall outside of the most plausible range of values

https://doi.org/10.1021/acs.energyfuels.5c00385
Energy Fuels 2025, 39, 6991−7011

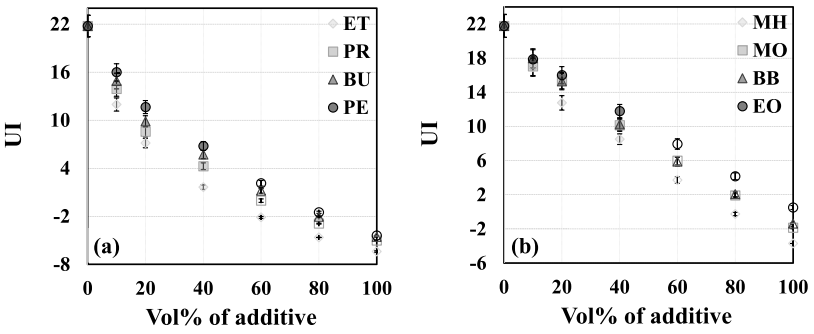

Figure 8. Evolution of the UI of fuel mixtures composed of the surrogate S8 with different alcohols (a) and esters (b) as a function of the vol % of oxygenate in the blends. Experimental points derived from SP measurements carried out with the blends comprising 10, 20, and 40 vol % of additives are depicted using close symbols, while data computed by means of the additivity rule defined in eq 4 for vol % of oxygenate of 60, 80 and 100% are represented by open symbols. Note that the error bars plotted on the graphs were drawn based on the experimental bias related to the SP measurements carried out using the VBA approach and extend to 95% confidence intervals (a mean bias value being considered to obtain the error bars of the computed points).

defined above. As for S4, it corresponds to the model fuel whose UI exhibits the highest discrepancy (RD of 48.24%) with respect to that of the Jet-A we tested. Finally, the sooting indexes of the other tested surrogates are relatively close (between ∼15 and ∼17), with RD values comprised between 17.98 (S6) and 27.95% (S1).

In further analyzing the results obtained, one can first note that the higher sooting propensity of S2 over S1 is consistent with the conclusions by ref 92, who compared the soot volume fractions measured in turbulent spray flames burning these two surrogates. Furthermore, the UI of S2 is slightly lower than that of Jet-A, which is also in line with the observations in ref 92, where it was noted that this model fuel leads to soot volume fractions similar to those measured when burning a Jet-A1 having aromatic and cycloparaffin contents (assessed by gas chromatography and mass spectrometry) lower than those of Jet-A as can be seen when comparing the compositions provided in refs 34 and 92. Regarding S5, which is similar to S8, except that isooctane was replaced with isocetane in the latter, its SP (25.5 mm) is 11.8% higher than that of Jet-A (22.8 mm) and 15.4% higher than that measured in ref 37 (22.1 mm) for the same model fuel. That the SP measured in this work for S5 differs from that estimated by ref 37 can first be explained by the fact that we assessed the smoke point using the VBA approach, which was demonstrated in Section 2.3 to be more precise than the manual method used by Dooley et al.[37] Furthermore, and due to the reproducibly of the manual method as specified in the ASTM D1322 standard,[32] the difference between two single and independent results obtained by different operators working in different laboratories on nominally identical test materials may be as large as 3.57 mm in the case of a fuel having a smoke point of 22.1 mm (which is the SP value reported in ref 37) in the normal and correct operation of the test method. Consequently, the smoke point difference observed when comparing the results reported in the present work and those in ref 37 may simply be related to the uncertainties encompassing the manual measurements carried out by ref 37. Finally, and even if considering an SP of 22.1 mm as proposed in ref 37, a UI of 18.63 would be obtained for S5, which would lead to an RD of 12.33%, versus 2.45% for S8. The latter surrogate would hence remain the best suited to mimic the UI of Jet-A. Concerning S3, S4, S6, and S7, the fact that their sooting tendency tends to diverge from that of the Jet-A analyzed in this work may be related to a high SP (as is the case of S4) and/or to low values of the $n + m/4 - p/2$ sum, thus leading to OESI values, and in turn UI ones, lower than those obtained with Jet-A or S8.

In conclusion, the above results show that the S8 blend performs better than the other tested surrogates in emulating the sooting propensity of the Jet-A we tested. It will therefore be considered in the following for blending with the various additives investigated in the present work. It is, however, not claimed that this model fuel should be considered universally valid or as representing the best formulation for capturing the main combustion features of kerosene. It is indeed reiterated that the focus here was only on the identification of a convenient surrogate that satisfactorily reproduces the sooting propensity of the Jet-A considered as a reference fuel herein. The aim was thus not to select or propose a comprehensive model fuel whose properties (ignition delay, heat release profile, viscosity, volatility, oxidation stability, etc.) would all match those of a commercial kerosene. That being said, the above results still showed that the S8 fuel presents multiple advantages. Indeed, and as mentioned in Section 2.1, its molecular weight, density, volumetric average boiling point, freezing point, and lower heating value are very similar to those of Jet-A (see Table 2). The smoke point of this model fuel, moreover, matches the values usually reported for Jet-A (see refs 37 and 41 as examples). To conclude, its relatively simple composition (it comprises 4 hydrocarbons whose chemistry is detailed in the literature (see ref 37 and references therein as well as ref 93, for instance) versus 5 components for S7 and 6 for S1 and S2) makes it an appealing candidate for the development of combustion kinetic models.

3.2. Analysis of the Soot Suppressing Effects of Alcohols and Esters Used as Additives to S8. The UI estimated during the analysis of a series of blends composed of the surrogate S8 with 10, 20, and 40 vol % of various alcohols are depicted in Figure 8a (data regarding esters which are plotted in Figure 8b being commented on further below in this section). Selected additives include ET, PR, BU, and PE, which are commonly considered to be mixed with kerosene and/or kerosene/diesel blends in compression ignition (e.g., ET in refs 13 and 14 and PE in ref 10), spark ignition (e.g., BU in ref 23), and gas turbine engines (e.g., PR, BU, and PE in ref 25), as explained in Section 1. For completeness, and in addition to measured points which are represented by close symbols in Figure 8, the UI of the fuels containing 60, 80, and 100% of oxygenate (depicted with open symbols) were computed by means of the additivity rule defined as per eq 4. To that end,

https://doi.org/10.1021/acs.energyfuels.5c00385
Energy Fuels 2025, 39, 6991−7011

we used the UI measured in Section 3.1 for S8. Furthermore, the UI of pure oxygenated molecules were taken equal to the means of the values derived from the implementation of eq 4 for the blends comprising 10, 20, and 40 vol % of additives for which measurements were carried out (i.e., $UI_{oxygenate} = (UI_{mixture} - UI_{S8} \cdot X_{S8})/X_{oxygenate}$).

As can be seen by looking at the plots of Figure 8a, the sooting tendency of the tested alcohols increases in the following order: ET < PR < BU < PE. This trend is actually in line with the observations from refs 56 and 94, who noted that the propensity of linear 1-alcohols to soot rises with an increasing number of carbon atoms (N_C) within the molecules. Besides, since fuel-bound oxygen is a key factor known to influence soot production,[95] it is essential to highlight the molecule features influencing the soot chemistry at play in order to further interpret the results obtained. To that end, we thus implemented the group contribution model developed in ref 56 following the procedure described in Section 2.5. Figure 9 depicts the correlation between the UI measured for all the

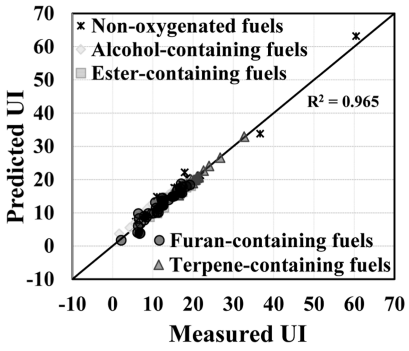

Figure 9. Correlation between measured UI and theoretical values computed using the group contribution model from ref 56.

fuels and fuel blends tested in the present work (including various nonoxygenated molecules comprised in the formation of the kerosene surrogates we tested (e.g., isooctane, decalin, toluene, tetralin, etc.)) and the values predicted by the model. As shown by the linear curve plotted in Figure 9, a strong positive correlation is obtained between the experimental and modeled results, with a high coefficient of determination (R^2 = 0.965), reflecting the dispersion of plotted data around the identity line. Of note, the computed R^2 is similar to that reported in ref 56, where a coefficient of determination of 0.972 was derived when analyzing the correlation existing between the UI issued from the extended database built therein and the values computed by means of the GCM. The slight reduction of the R^2 noted herein can still be explained by the fact that only 96 points were used to plot the curve of Figure 9 versus more than 500 in ref 56. Overall, the good ability of the GCM to properly predict the sooting behavior of the fuel blends tested in this work, including alcohol-containing ones depicted using diamonds in Figure 9 (data related to other oxygenates being discussed further below), demonstrates the consistency of the model proposed in ref 56, as also highlighted by ref 57. This model can therefore be considered as an interesting simulation tool allowing to better understand the sooting behavior of oxygenated additives while providing insights into how their chemical structure affects soot formation as exemplified below.

By analyzing the contributions C_j of the structural fragments composing the tested alcohols, one can first note that the reason for the higher UI of PE over BU (whose sooting tendency is itself higher than that of PR and ET) can be traced to the addition of one $[C-(C)_2(H)_2]$ fragment, which is characterized by a positive contribution of +0.795 (see Table 1 of ref 56), each time the N_C of linear 1-alcohols increases by one. On the other hand, the fact that the 4 considered alcohols drastically reduce the propensity to soot of the S8 fuel when they are added to this surrogate can be explained by the presence of the $[C-(C)(H)_3]$, $[C-(O)(C)(H)_2]$, and $[O-(C)(H)]$ fragments whose combination leads to a strong negative contribution of −3.384 and which are all included in the structure of ET, PR, BU, and PE.

As far as the sooting tendency of the ester-containing fuels is concerned, Figure 8b reports the UI measured (vol % between 10 and 40%) and computed (vol % between 60 and 100%) for the blends containing MH, MO, BB, and EO. As mentioned in Section 1, these compounds were selected for blending with S8 since esters have recently attracted particular interest for mixing with kerosene and kerosene/diesel blends (see refs 12, 20, 21, 58, and 59 as examples). The results plotted in Figure 8b first show that the UI of the tested esters increases in the following order: MH < MO < BB < EO. Here again, the slightly higher sooting tendency of MO over MH is consistent with the results from refs 56 and 94, who concluded that the higher the N_C, the higher the propensity of methyl esters to soot. According to the C_j of the groups composing MO and MH, this trend can be related to the addition of one $[C-(C)_2(H)_2]$ fragment having a positive contribution of +0.795, as mentioned above, each time the N_C value increases by one. The GCM, moreover, traces the higher UI of EO as compared to MO to the substitution of the methyl group of the latter by an ethyl group. As a result, the $[C-(O)(H)_3]$ fragment of MO, whose contribution is negative (−0.619[56]), is replaced by the combination of the $[C-(O)(C)(H)_2]$ and $[C-(C)(H)_3]$ groups, whose combined C_j lead to a positive value of 0.166.[56] Finally, although containing only 8 carbon atoms, BB is still shown in Figure 8b to soot more than MO, whose N_C is 9. This observation is, however, in line with the conclusions from ref 94, who noted that the sooting tendency of butyl esters was close to that of methyl or ethyl esters having 2 to 3 more carbon atoms in their molecular chain. Six-center reactions impeding the soot-suppressing effect of esters through the trapping of two oxygen atoms by a single carbon likely explain this specific behavior. These reactions, which are absent in the case of methyl esters, while producing a soot precursor (ethylene) similar to that issued from the combustion of *n*-alkanes in the case of ethyl esters, are alternatively likely to convert the carbon chain on the ether side of butyl esters into fragments, promoting soot formation more than ethylene.

In conclusion, all of the tested alcohols and esters have a sooting tendency significantly lower than that of the S8 fuel. While the considered C_2 to C_5 alcohols are quite logically characterized by a higher soot-reducing potential than the C_7 to C_{10} esters (the number of $[C-(C)_2(H)_2]$ fragments contributing to soot production being lower in the case of ET, PR, or BU), the latter still present some interesting features, including a higher density (between 869 kg/m^3 for BB and 885 kg/m^3 for MH versus values ranging from 789 kg/m^3 for ET to 811 kg/m^3 for PE) and relatively high LHV (between 30.2 MJ/kg for MH and 33.2 MJ/kg for EO versus 27 MJ/kg for ET, for instance). Furthermore, despite its

https://doi.org/10.1021/acs.energyfuels.5c00385
Energy Fuels 2025, 39, 6991−7011

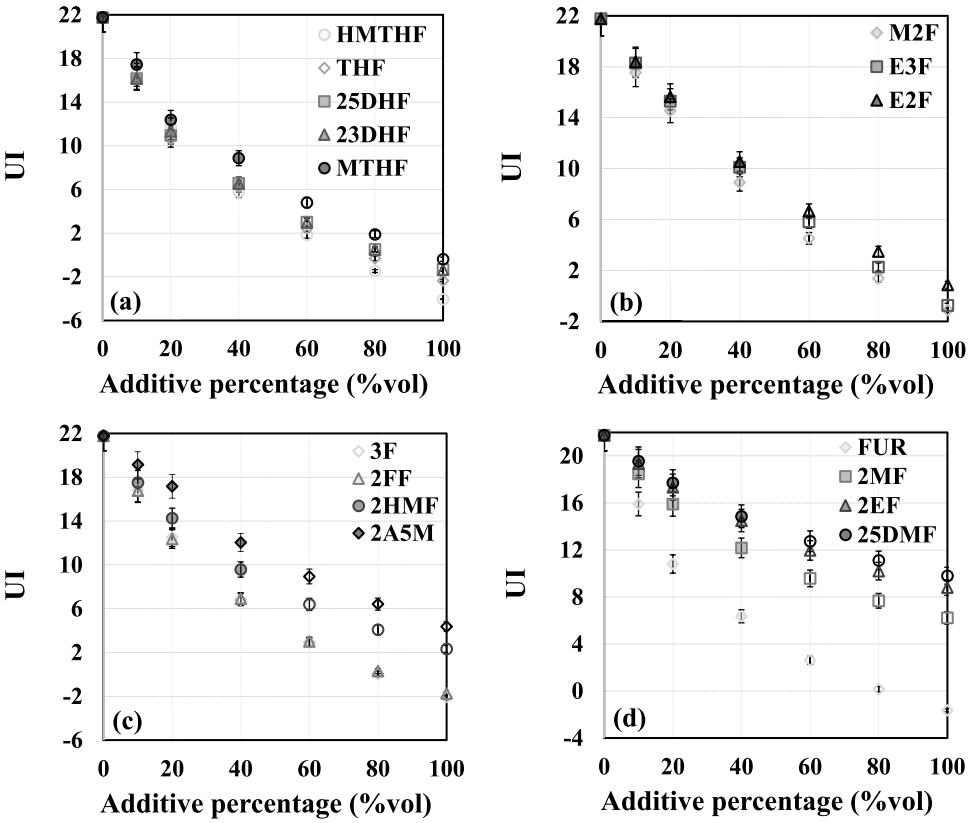

Figure 10. Evolution of the UI of fuel mixtures composed of the surrogate S8 with different furans, including hydrogenated furans (a), furans with ester groups (b), furans with other oxygenated groups (c), furan and alkyl-substituted furans (d), as a function of the vol % of oxygenate in the blends. Experimental points are depicted using close symbols while computed ones are represented by open symbols (see the caption of Figure 8). Finally, error bars were drawn based on the experimental bias related to the SP measurements carried out using the VBA approach and extend to 95% confidence intervals.

somewhat high sooting tendency compared to the other tested oxygenates, BB is regarded as a promising additive since it is fully compatible with aviation kerosene.[58] It notably exhibits a distillation profile, a viscosity, and a flash point similar to those of Jet A-1.[58,59] Similarly, EO, with an UI that is slightly higher than that of BB, also presents remarkably similar properties to Jet A-1,[59] thus making BB and EO interesting aviation biofuels. Conversely, alcohols, such as butanol, typically distill out of the kerosene fuel at low temperatures while having cloud and flash points that are out of the required specifications. That said, they could still be considered for other applications in compression or spark-ignition engines as mentioned above and in Section 1.

3.3. Analysis of the Soot Suppressing Effects of Furans and Terpenes Used as Additives to S8. Figure 10 depicts the UI estimated for different blends comprising the surrogate S8 to which 10, 20, and 40 vol % of various furans were added. The sooting index values assessed in the cases of THFs and DHFs (i.e., HMTHF, THF, 25DHF, 23DHF, and MTHF) are plotted in Figure 10a, while those relating to furans containing an ester group (i.e., M2F, E2F, and E3F) and other oxygenated groups (i.e., 3F, 2FF, 2HMF, and 2A5M) are detailed in Figure 10b and c, respectively. Finally, the results obtained with furan and alkyl-substituted furans (2MF, 2EF, 25DMF, and FUR) are reported in Figure 10d.

As stipulated in Section 1, these molecules were especially considered due to the recent growing interest in the use of furans as jet fuel substitutes.[29] Of note, the sooting propensity of M2F, E2F, E3F, 3F, and 2A5M has hardly ever (if at all) been characterized in the literature to the best of the authors' knowledge, which explains the reasoning behind our integration of these molecules in the experimental data set processed herein. As for THFs and DHFs, they were considered due to their energy density, which is higher than that of their furan counterparts.[96] They, moreover, exhibit relatively low sooting tendencies, as exemplified in ref 96, where HMTHF was shown to soot slightly more than PR despite its three extra carbon atoms. For their part, 2FF and 2HMF were selected because of the oxygenated side chains they contain, which makes them interesting soot-suppressing additives.[96] As for 2MF, it has different advantages over more conventionally used short-chain alcohols such as ET, which was tested in Section 3.2. These notably include its insolubility in water, which could make it, as well as its blends with other fuels, more stable. It also has a lower latent heat of vaporization, which can alleviate the engine cold-start problem, as well as a higher energy density likely to enhance engine efficiency and decrease fuel consumption. Furthermore, 2MF has a higher research octane number than gasoline[97] while being associated with similar and even lower emission levels when being burnt in spark-ignition engines (see ref 29 and references therein). Similarly, 2MF and 25DMF have good knock suppression abilities as well as beneficial behaviors with respect to soot emission.[98]

Note that as was done for alcohols and esters in Section 3.5, the group contribution model developed in ref 56 was used to interpret the sooting trends relating to furans and terpenes. That being said, and as mentioned in Section 2.5, the

https://doi.org/10.1021/acs.energyfuels.5c00385
Energy Fuels 2025, 39, 6991−7011

Table 7. List of Functional Groups Comprised in the Studied Furans and Terpenes, Together with Their Contribution to the UI[a]

j	group	C_j	j	group	C_j
furans			97	$[CO-(C_f)(H)]$	−1.896
89	$[C-(C_f)(H)_3]$	3.911	98	$[C_f-(CO)]$	0.811
90	$[C_f-(O)(C)]$	1.254	99	$[CO-(O)(C_f)]$	3.306
91	$[C_f-(H)]$	−0.723	100	$[CO-(C_f)(C)]$	0.218
92	$[O-(C_f)_2]$	0.924	terpenes		
93	$[C_f-(O)(H)]$	−0.578	69	$[C-(O)(C_d)(C)_2]$	−2.265
94	$[C-(C_f)(C)(H)_2]$	9.429	101	$[C_d-(C_d)(C)]$	9.162
95	$[C-(O)(C_f)(H)_2]$	5.100	102	$[CO-(C_d)(H)]$	−5.375
96	$[C_f-(CO)(O)]$	1.574			

[a]Note that the values of the group index j were set to be consistent with the formalism adopted in ref 56 while pursuing the fragment numbering proposed therein.

contributions C_j of different groups composing these molecules were unknown. The few C_j reported in ref 56 for the fragments specific to furanic molecules (namely, groups j = 89 $[C-(C_f)(H)_3]$, j = 90 $[C_f-(O)(C)]$, j = 91 $[C_f-(H)]$, j = 92 $[O-(C_f)_2]$, and j = 93 $[C_f-(O)(H)]$) were, moreover, derived from the processing of a relatively limited data set comprising 7 molecules versus 16 in the present work. Since the larger the database, the greater the frequency of occurrence of the fragments and the more relevant the derived sooting contribution factors, updated C_j values were thus computed for the above-listed groups. Furthermore, the smoke points of THF, 23DHF, 25DHF, FUR, MTHF, 2MF, and 25DMF listed in ref 56 were issued from measurements carried out using a setup integrating a servomotor to rotate the fuel tank nut of the SP lamp. The piezo inertia actuator used herein, however, led to more precise results, as exemplified by the experimental biases and relative differences reported in Section 2.3.3, which were shown to be lower than those computed in ref 52. The smoke points of THF, 23DHF, 25DHF, FUR, MTHF, 2MF, and 25DMF were therefore measured anew to potentially refine the obtained data. In the end, the updated C_j values reported in Table 7 for groups j = 89, 90, 91, 92, and 93 were very close to those previously inferred in ref 56. The contributions of groups j = 90, 91, and 93 indeed remained similar, with values of 1.254, −0.723, and −0.578, respectively, instead of 1.045, −0.695, and −0.551 in ref 56. As for the C_j of groups j = 89 and 92, they changed from 2.076 and −0.702 to 3.911 and 0.924, respectively. The preceding notwithstanding, the variations observed still fall within the credible intervals defined in ref 56 (see Figure 3 therein). Furthermore, the fact that the occurrence of group j = 92 in the new data set processed herein was multiplied by 3.7, for instance, especially explains why the refined contributions in Table 7 differ slightly from those previously found in ref 56. Regarding groups j = 94 to 100, their sooting contributions were determined following the methodology described in Section 2.5. Since some groups were systemically combined, only global contributions were hence estimated for the following couples: j = 96 + j = 97, j = 96 + j = 99, j = 96 + j = 100, j = 97 + j = 98, and j = 98 + j = 99. Inferring individual contributions for groups j = 96 to 100 then implied setting constraints allowing us to downsize the research area while guiding the optimization algorithm. To that end, and in agreement with the conclusions from refs 47, 55, and 56, the soot-promoting effect of unsaturated fragments was considered to be higher than that of their saturated counterparts (as verified in ref 56, where the contribution of the $[C-(C_t)(H)_3]$ group was found to be higher than that of the $[C-(C_d)(H)_3]$ fragment, which was itself higher than the sooting propensity of the group $[C-(C)(H)_3]$). In particular, it was found in ref 56 that groups containing carbon atoms involved in furanic cycles (i.e., C_F) tended to generate more soot than their counterparts integrating single or double-bonded carbons, as exemplified by the C_j of group j = 89 $[C-(C_f)(H)_3]$, which was shown to be higher than that of group j = 5 $[C-(C_d)(H)_3]$, itself higher than the contribution of group j = 1 $[C-(C)(H)_3]$. Consequently, as examples, the following constraints were set: C_j of group j = 97 $[CO-(C_f)(H)] > C_j$ of group j = 18 $[CO-(C)(H)]$, C_j of group j = 99 $[CO-(O)(C_f)] > C_j$ of group j = 25 $[CO-(O)(C)]$, and C_j of group j = 100 $[CO-(C_f)(C)] > C_j$ of group j = 19 $[CO-(C)_2]$. This led to the estimation of the contributions listed in Table 7, noting that the latter is not to be deemed universally valid. As explained in refs 55 and 56 as examples, large uncertainties indeed encompass the inference of sooting contribution factors from the processing of measured SI. The different C_j proposed herein still allow computing theoretical UI matching their experimental counterparts, as shown in Figure 9, which thus tends to illustrate the overall consistency of our updated GCM model. Finally, the contributions of the groups j = 101 and 102 which are present in some studied terpenes will be commented on below when analyzing the results obtained with MC, GNA, GNO, CTL, LNL, and 18CL.

As can be seen by looking at the results reported in Figure 10a, the sooting tendency of the tested hydrogenated furans increases in the following order: HMTHF < THF < 23DHF−25DHF < MTHF. The fact that dihydrofurans soot more than THF is consistent with the small mole fractions of cyclic unsaturated hydrocarbons issued from its combustion, as illustrated in ref 99 and explained in ref 56. THF is indeed mainly consumed by H-abstractions from the carbon atoms bonded to the oxygen atom by flame-propagating radicals, which leads to the production of a tetrahydrofur-2-yl radical. Alternatively, dihydrofurans generate dihydrofuryl radicals, which are converted into furan together with $CH_2CHCHCHO$ and $CHCHCH_2CHO$ radicals, hence, enhancing the amount of soot precursors formed. In accordance with the observations from ref 96, the plots of Figure 10a also show that HMTHF exhibits the lowest sooting tendency, which can be traced to its specific molecular structure consisting of a low sooting THF ring substituted with a hydroxymethyl group (j = 21 $[O-(C)(H)]$) having a negative sooting contribution of −3.550. As for the UI of the blends containing 23DHF and 25DHF, they are almost superimposed in Figure 10a. 25DHF is still found to be ∼3% more sooting than 23DHF, which can be

https://doi.org/10.1021/acs.energyfuels.5c00385
Energy Fuels 2025, 39, 6991−7011

related to a reduced production of reactive radicals during its oxidation.[97] According to the GCM predictions, the slightly higher sooting propensity of 25DHF over 23DHF can be linked to the position of the carbon functional groups presenting double bonds in the structure of these molecules. The latter indeed induces a small increase of the UI due to the involvement of different fragments including group j = 44 [C−(O)(C_d)(H_2)] in 25DHF, whose contribution is greater than that of group j = 45 [C_d−(O)(H)] present in 23DHF (see ref 56 for details of the contribution values relating to groups j = 1 to 88). Finally, the higher sooting propensity of MTHF over THF, also observed in refs 56 and 96, can be related to the replacement of the group j = 13 [C−(O)(C)(H_2)] in THF by the coupling of groups j = 1 [C−(C)(H_3)] and j = 14 [C−(O)(C_2)(H)] in MTHF whose combined sooting contribution is higher than that of the [C−(O)(C)(H_2)] fragment.

As for the furans which are substituted with an ester group, Figure 10b shows that their propensity to soot follows the order M2F < E3F < E2F. Since to the best of the authors' knowledge, no previous work truly sought to characterize the sooting tendency of these molecules, no direct comparison with results issued from the literature can thus be made. Nevertheless, our updated GCM still allows interpreting observed trends and notably highlights that the higher UI of E2F over M2F is directly related to the replacement of the ethyl ester in the former (the combination of groups j = 1 [C−(C)(H_3)] and j = 13 [C−(O)(C)(H_2)] being associated with a positive sooting contribution of 0.166) by a methyl ester (for its part characterized by the negative C_j (−0.619) of group j = 12 [C−(O)(H_3)]). Regarding the sooting behavior difference between E2F and E3F, the latter appears to be influenced by the position of the branching. Actually, the results obtained tend to indicate that the sooting propensity of ethyl furoates slightly decreases as the ester group is pulled away from the oxygen in the furan ring, perhaps due to the breaking of the molecules into smaller fragments that are less efficient in promoting soot.

The data from Figure 10c then show that 2A5M soots more than 2HMF, which itself soots more than 2FF and 3F. Although, to the best of the author's knowledge, no SI values are reported in the literature for 3F and 2A5M, the authors of ref 96 still observed that 2FF was less sooting than 2HMF, which agrees with the results obtained in the present work. This trend can be explained by the nature of the group composing the branching. Indeed, and as noted in ref 56, the propensity to soot of oxygenated functional groups tends to increase in the following order: ester < carbonyl < hydroxyl. Since both 3F and 2FF contain a carbonyl functional group (characterized by the presence of the fragment j = 97 [CO−(C_f)(H)], which has a negative C_j value as illustrated in Table 7), these molecules are thus less sooting than 2HMF, whose branching notably comprises groups j = 21 [O−(C)(H)] and j = 95 [C−(O)(Cf)(H_2)], whose combined contribution is positive. Similarly, and although integrating a low sooting [C−(CO)(H_3)] fragment, 2A5M also includes the fragment j = 89 [C−(Cf)(H_3)], whose C_j is quite high, hence explaining its sooting behavior. Finally, it is noteworthy that the UI inferred for 2FF is slightly higher than that of 3F, as was the case when comparing the sooting propensity of E2F and E3F. This therefore tends to corroborate the above observation regarding the fact that the farther the branching is from the oxygen in the furan ring, the lower the sooting tendency.

Figure 10d finally shows that the UI of the 4 furans whose results are reported therein increases in the order: FUR < 2MF < 2EF < 25DMF. The fact that FUR, whose UI is quite close to that of the two tested DHFs (see Figure 10a), soots less than 2MF, 2EF, and 25DMF is in line with the observations from refs 56 and 96. This behavior can be traced to the absence of methyl and ethyl substitutions in this molecule, contrary to 2MF and 25DMF, which contain one and two relatively sooting [C−(C_f)(H_3)] groups (see Table 7), respectively, and 2EF, which integrates an ethyl substitution notably composed of groups j = 1 and 94, whose combined contribution is 7.649. The fact that 2EF soots more than 2MF but less than 25DMF, its isomer, is moreover consistent with the conclusions from ref 96. According to the predictions from the GCM, this trend may be related to the fact that the UI increases by 5.165, when adding a methyl substitution to a carbon atom adjacent to the oxygen of the furanic cycle (sum of the contributions of groups j = 89 and 90), versus 8.903, when adding an ethyl side chain (combination of the contributions of groups j = 1, 90, and 94), hence justifying the higher propensity to soot of 2EF over 2MF. On the other hand, adding two methyl substitutions instead of an ethyl one leads the UI to increase by 10.33 versus 8.903, thus explaining why 25DMF soots more than 2EF.

As far as terpenes are concerned, the UI measured when analyzing the blends composed of the surrogate S8 with 10, 20, and 40 vol % of MC, GNA, GNO, CTL, LNL, and 18CL (see Table 3) are plotted in Figure 11. As mentioned in Section 1,

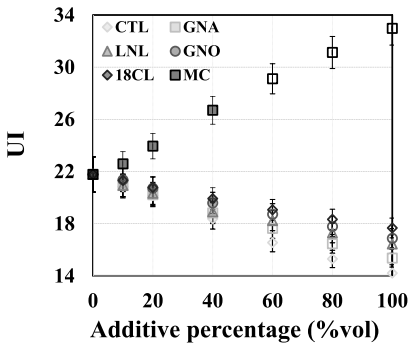

Figure 11. Evolution of the UI of fuel mixtures composed of the surrogate S8 with different terpenes as a function of the vol % of additive in the blends. Experimental points are depicted using close symbols, while computed ones are represented by open symbols (see the caption of Figure 8). Finally, error bars were drawn based on the experimental bias related to the SP measurements carried out using the VBA approach and extend to 95% confidence intervals.

these molecules were chosen due to their potential use as jet fuel substitutes, to their relatively low sooting propensity as compared to Jet-A,[30] to their branched structures leading most terpenes to exhibit favorable cold weather properties,[30] and to their high energy density, as exemplified in ref 100 for MC, GNO, and LNL. The data depicted in Figure 11 first show that the sooting tendency of the tested additives increases in the following order: CTL < GNA < LNL < GNO < 18CL < MC. This is actually in agreement with the conclusions from ref 30, except for the case of MC, which is highly sooting herein o be similar to that of GNO in ref 30. When analyzing the obtained results in greater detail, it can first be noted that the low UI values obtained with GNA and CTL are consistent with the fact that they contain a carbonyl group, which is well known

https://doi.org/10.1021/acs.energyfuels.5c00385
Energy Fuels 2025, 39, 6991−7011

for its significant soot-suppressing effect (see above). The higher UI of GNA over CTL is, moreover, in line with the predictions of the GCM. The latter indeed traces this trend to the presence of two double-bonded carbons in GNA, versus one in CTL, noting that the greater the degree of unsaturation, the higher the sooting tendency.[56] As for the higher sooting propensity of LNL over GNA, it can be explained, according to the GCM, by the presence of two highly sooting [C_d−(C)(H)] fragments in LNL, in addition to the presence of a hydroxyl group j = 21 [O−(C)(H)], whose sooting contribution (−3.550) is greater than that of the carbonyl group j = 102 composing GNA (see Table 7). This specific trend, moreover, agrees with the fact that 3-alcohols are known to soot more than aldehydes for a given N_C,[94] although the structure of the considered molecules should obviously also be taken into account, as is done above. The higher UI measured with LNL and GNO as compared to CTL and GNA can also be explained by the presence of a hydroxyl group in linalool and geraniol, which soots more than the carbonyl group from citronellal and geranial. Finally, the GCM also properly predicts the fact that CTL and GNA are less sooting than 18CL, which notably integrates two highly sooting groups j = 15 [C−(O)$(C)_3$]. Nevertheless, even though the updated group increment model used herein proved to perform globally well, some discrepancies between the measured and predicted UI still exist. For instance, and in agreement with the results from ref 30, we found that the UI of 18CL was slightly higher than that of GNO (17.67 versus 16.89). The model, however, leads to computed UI values of 16.24 and 18.29 for 18CL and GNO, respectively. As previously noted in ref 56, the reason for this can be traced to the presence of the fragment j = 22 [O−$(C)_2$] in 18CL, which is also present in linear ethers. The fact that the contribution for this specific group was derived without a distinction being made between groups present in linear or cyclic ethers is thus likely to give rise to biases due to various effects, including ring strains, for instance, which are not considered. This hence prevents the GCM from properly capturing the sooting behavior of some cyclic compounds, as also noted in the case of the blends containing THFs and DHFs whose predicted UI were found to differ from measured ones by 23%, on average. Furthermore, the GCM predictions were also found to significantly overstate the sooting propensity of LNL due to the significant uncertainty surrounding the contribution of the group j = 69, whose occurrence was 1 in ref 56. We therefore reprocessed the results obtained in ref 56, as previously done for groups j = 89 to 93 (see above), while considering LNL in the database to infer the updated contribution of the fragment j = 69 reported in Table 7. This led to an estimation of a theoretical UI of 15.33 instead of 26.46 for LNL, which is much closer to the measured value of 16.39 (see Figure 11). Additional molecules integrating this fragment with a low occurrence should, however, be tested in the future to further improve the estimation of its sooting contribution. Finally, it is noteworthy that identical YSI were measured for MC and GNO in ref 30, while the former was found to be much more sooting in the present work. To further confirm this contradictory trend, we performed additional measurements with pure MC. This notably allowed to validate of the consistency of the UI inferred when processing the results obtained with the S8/MC blends using the additivity rule depicted in eq 4 (see Section 3.2) while excluding the potential influence of synergistic effects. The obtained results then confirmed that the UI of MC was significantly higher than that of GNO, contrary to what was found by ref 30. The GCM, moreover, predicts a UI of 32.923 which, here again, matches the value we measured for MC. In their detailed analysis, the authors of ref 30 reported that the YSI of MC (103.6) was much lower than that of its isomer, β-ocimene (referred to as b-OM (213.6)), whose structure is similar, except for the position of one of its C−C double bonds. To explain this specific trend, it was suggested in ref 30 that b-OM would undergo non-nearest neighbor interactions (denoted NNIs[55] or NNNIs[30]) enhancing soot formation. This would especially explain why their GCM failed to properly simulate the sooting behavior of this molecule (a value of 89.6 being indeed assessed instead of 213.6) since NNNIs are intrinsically not taken into account in GCMs derived from the approach proposed by Cohen and Benson.[53] When computing the UI of b-OM using our model, we still found a value of 43.048, which actually accounts for the higher propensity to soot of b-OM over MC. Furthermore, when plotting the variation of the YSI measured by ref 30 as a function of the UI computed with our GCM for CTL, GNA, LNL, GNO, 18CL, and b-OM (results not reported, for brevity), one obtains a strong positive correlation with an R^2 of 0.98. Since the GCM used herein is able to properly account for the higher sooting propensity of b-OM over CTL, GNA, LNL, GNO, and 18CL, one could hence exclude the existence of potential NNNIs. Finally, it was found in ref 30 that the YSI of MC was, respectively, similar to and lower than the values obtained for GNO and 18CL, which is not truly consistent with the fact that MC does not contain any soot-suppressing oxygenated fragment, unlike GNO and 18CL, while having more C−C double bonds. As an example, MC typically includes groups j = 42 and 7, whose combined contribution reaches 9.004, at the end of its chain, while GNO instead integrates groups j = 21 and 44, which are characterized by a strong soot-suppressing effect, as exemplified by the corresponding contributions which amount to −12.122. All these observations therefore tend to confirm the higher tendency to soot of MC over the other tested terpenes. Leading complementary analyses aimed at better interpreting the reasons explaining the diverging trend highlighted with respect to MC would therefore be beneficial. These could include a difference in combustion media, noting that the authors in ref 30 used a methane flame doped with 1000 ppm of the tested molecule, while in the present work, MC was burnt pure or in mixtures at high vol % in an SP lamp.

In conclusion, all of the tested furans were found to reduce the sooting propensity of S8 when being added to this surrogate. THFs and DHFs were especially shown to have low UI values comprised between −0.388 (MTHF) and −4.052 (HMTHF). Similarly, negative UI of −2.066, −1.743, and −1.652 were measured for 3F, 2FF, and FUR, respectively. This thus makes these molecules interesting soot-suppressing additives, especially as compared to short-chain alcohols such as PR, whose UI is only slightly lower than that of HMTHF, for instance (see Section 3.2). THFs with short side chains, moreover, exhibit desirable ignition features, hence making them suitable candidates for gasoline replacement.[97] Regarding the other tested furans with higher sooting propensities (e.g., 2HMF, FUR, 2MF, 2EF, and 25DMF), they still present interesting properties, including a good knock suppression ability, hence making them compliant with spark ignition engine applications[97] while allowing to reduce engine particulate matter emissions, as exemplified with 2MF in ref

https://doi.org/10.1021/acs.energyfuels.5c00385
Energy Fuels 2025, 39, 6991−7011

98. As for terpenes, only MC (the only nonoxygenated additive tested herein) was found to soot more than the S8 surrogate. Besides, while being more sooting than the tested C_2 to C_5 alcohols, C_7 to C_{10} esters, and C_4 to C_7 furans, the other considered terpenes still have interesting features, including high energy densities (e.g., 45.96 MJ/kg for MC, 40.47 MJ/kg for GNO, and 40.34 MJ/kg for LNL[100]), in addition to branched structures promoting favorable cold weather properties.[30]

3.4. Analysis of the Sooting Behavior of Pyrolysis Oils Used as Additives to S8. Figure 12 depicts the UI estimated for the blends composed of the surrogate S8, to which 10, 20, and 40 vol % of SW and S POs were added.

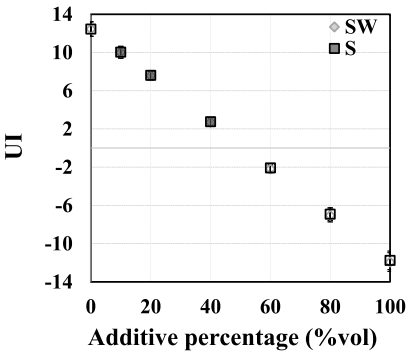

Figure 12. Evolution of the UI of fuel mixtures composed of the surrogate S8 with W and SW POs as a function of the vol % of additive in the blends. Experimental points are depicted using close symbols, while computed ones are represented by open symbols (see the caption of Figure 8). Error bars were drawn based on the experimental bias related to the SP measurements carried out using the VBA approach and extend to 95% confidence intervals. Finally, note that the UI measured for an additive content of 0 vol % is lower than that reported in Figures 8, 10, and 11 since it corresponds here to the UI of the S8/surfactant/methanol blends used for the emulsification process (see Section 2.1).

The obtained results first show that both POs exhibit relatively similar sooting behaviors, although the S PO is still found to soot slightly more than the SW one. Furthermore, although being composed of relatively complex mixtures of hydrocarbons and oxygenated molecules notably comprising phenols, ketones, and furans (see Section 2.1), the UI estimated for pure POs (i.e., −11.93 and −11.75 for SW and S POs, respectively) are still lower than those of the other additives considered in Sections 3.2 and 3.3. It is, however, noteworthy that assessing the UI of the POs by means of eq 4 requires computing the mole fraction of each component of the blend. To that end, we thus used the molecular weight (MW) reported in Table 4, noting that this parameter is subject to a relatively large uncertainty, as exemplified in ref 101, where the molecular weight of POs was shown to significantly vary from one study to another. A sensitivity analysis dealing with the impact of MW on the assessed UI values was therefore conducted. We then noted that a ±25% variation of the selected MW values typically led to UI comprised between −14.37 and −10.36 for the SW PO versus −14.96 and −9.78 for the S one (these uncertainty ranges being depicted by means of error bars in Figure 13, which will be commented on in Section 3.5). As a consequence, even while considering the possible variations encompassing the MW values considered in computing the UI of pure POs, their propensity to soot is still shown to be lower than that of the other additives tested in the present work. The high water contents of the tested POs (22.74 and 29.05 wt % for SW and S, respectively) are actually likely to explain this specific trend. Indeed, while studying the effect of water emulsification on the flame structure, combustion efficiency, and exhaust emissions in a laboratory spray combustor, the authors of ref 102 showed that the total amount of soot yielded in spray flames was significantly reduced when increasing the water fraction of *n*-dodecane/water emulsions. This trend was, moreover, observed even at low levels of water addition, with a reduction of ∼45% of the soot yield when increasing the water content from 0 to 5 wt %. According to ref 102, this phenomenon can be traced to an enrichment of water vapor in the fuel-rich

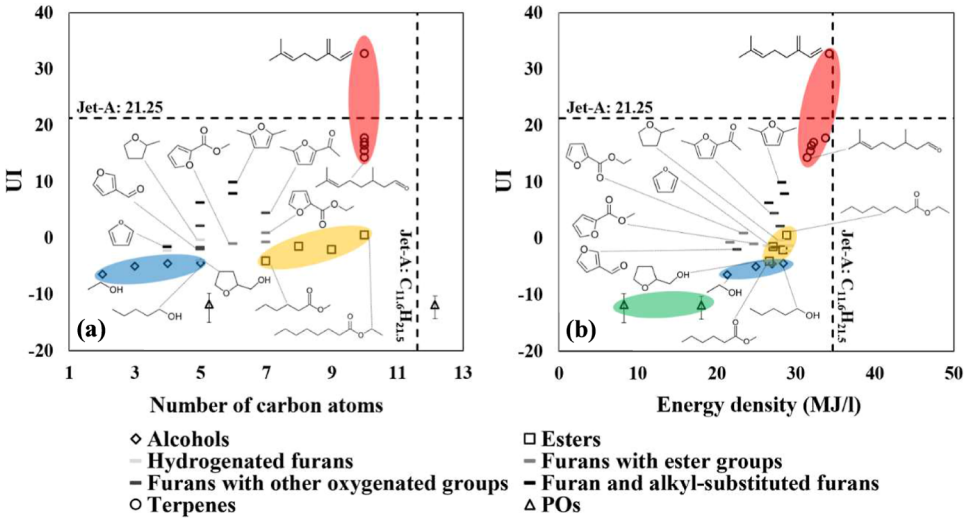

Figure 13. UI of the different fuels tested in the present work as a function of their N_C (a) and energy density (b). Note that black dotted lines denote the properties of Jet-A, while the green, blue, orange, and red regions cover the points corresponding to POs, alcohols, esters, and terpenes, respectively. Note also that the energy density values were computed by multiplying the lower heating value (LHV) of each fuel by the density, noting that the procedure detailed in ref 103 was used to convert the HHV values of POs into LHV.

https://doi.org/10.1021/acs.energyfuels.5c00385
Energy Fuels 2025, 39, 6991−7011

regions of the flame together with a reduction of the temperature, which both contribute to reducing soot formation in the gas phase. Furthermore, the addition of water contributes to an increase in OH radicals, enhancing soot oxidation. That being said, despite their surprisingly low UI, tested POs may face major challenges when it comes to being used in practical combustors notably due to their low pH and HHV (see Table 4).

3.5. Synthesis of Obtained Results and Concluding Discussion. To conclude this work, in Figure 13, we plotted the UI of the different fuels analyzed in previous sections as a function of their N_C (see Figure 13a) and energy density, hereafter referred to as "ED" (see Figure 13b). As can be seen, all the considered additives, with the exception of the pyrolysis oil produced from SW, have a lower N_C than Jet-A (see Figure 13a), while exhibiting a lower energy density (see Figure 13b). Furthermore, and with the exception of myrcene, all the tested fuels have a propensity to soot, which is lower than that of Jet-A. In agreement with the trends reported in Sections 3.2, 3,3, and 3.4, the soot-suppressing effect of the additives follows the general trend: POs > alcohols > esters > furans > terpenes. While enabling the identification of low-sooting fuels providing a strong lever for reducing soot emissions at the exhaust of combustion systems conventionally fueled with kerosene, the data plotted in Figure 13b also show that the additives having the lowest sooting tendencies generally correspond to those having the lowest ED, the latter property decreasing in the order: terpenes > esters > alcohols > POs. As for the furanic species, their energy content strongly depends on their molecular structure and spans a range of ED values going from that of alcohols (furans with ester groups) to that of esters (alkyl-substituted furans). Although sooting more than POs, alcohols, esters, and furans, terpenes still have an energy density similar to that of Jet-A while offering soot reduction benefits (except in the case of MC). This thus makes them potentially promising additives for blending with petroleum-derived kerosene as is the case of BB and EO, which present properties remarkably similar to those of Jet A-1. Conversely, and despite being characterized by very low UI values, POs exhibit high water content, low pH and ED, and high viscosity in addition to poor stability and insolubility in traditional liquid fuels.[104] This hence prevents POs from being used without first improving their properties through the implementation of catalytic treatments aimed at optimizing the selectivity toward some desired products in order to produce upgraded pyrolysis oils.[104−107]

4. CONCLUSIONS

This work explored the potential soot-suppressing effect of 32 different additives identified in the literature as promising candidates to be blended with kerosene. To ease the analysis of the impact of the structure of the tested fuels on the soot chemistry, a simplified model fuel aimed at emulating the sooting tendency of a commercial Jet-A was considered as a base fuel instead of kerosene. The unified index (UI) values of the burnt mixtures were then analyzed by means of a group contribution model (GCM) whose predictive capability was extended through the proposal of submodels suitable for predicting the propensity to soot of furans and terpenes. Based on the results obtained, the following conclusions can be drawn:

- The comparison analysis of the smoke point (SP) measurement approaches commonly used in the literature shows that the fuel uptake rate measurement with threshold imaging (FURTI) and vision-based algorithm-aided (VBA) automated methods are more precise and accurate than the ASTM D1322 manual method. Although the mean experimental biases and relative errors estimated with the FURTI and VBA methods are relatively similar, the VBA approach was still found to perform slightly better while being easier to implement and leaving the operator little room regarding the interpretation of measured data.
- Among the 8 kerosene surrogates tested herein, the blend composed of 40.41 mol % *n*-dodecane, 7.28 mol % mesitylene, 29.48 mol % isocetane, and 22.83 mol % *n*-propylbenzene was found to be the most adapted to reproduce the sooting propensity of the commercial Jet-A considered in this work. In addition to comprising only 4 hydrocarbons, whose chemistry is detailed in the literature, this simple model fuel also has a molecular weight, density, volumetric average boiling point, freezing point, and lower heating value quite close to those of Jet-A, which thus makes it a convenient comprehensive surrogate.
- The GCM previously developed in ref 56 has been extended to integrate new sooting contributions which are specific to 15 functional groups entering into the composition of furans and terpenes. This improved GCM, which is one of the most comprehensive ever built, now integrates 102 fragments whose propensities to soot were assessed based on an extensive set of sooting index values issued from the analysis of 521 different molecules.
- As for the sooting propensity of the pure molecules tested as additives, it was found to follow the general trend: C_2-C_5 alcohols < C_7-C_{10} esters < C_4-C_7 furans < C_{10} terpenes. Although this general trend shall be helpful in identifying interesting oxygenated additives for use in internal combustion engine applications, further investigation shall be done in quantifying the fuel performances in such applications, as was done in ref 108, for instance. Besides, and while confirming that the sooting tendency of alcohols and methyl esters increases with the number of $[C-(C)_2(H)_2]$ fragments added to the carbon chain, the results we obtained also showed that butyl butyrate soots more than methyl octanoate, despite its lower number of carbon atoms (N_C), which has been traced to the existence of six-center reactions. As for furans, measured UI showed that hydrogenated furans tend to soot less than furans with oxygenated groups, which themselves soot less than alkyl-substituted furans. According to the GCM, the low UI of hydrogenated furans can be related to the presence of low sooting fragments in these compounds (such as $[O-(C)(H)]$ and $[O-(C)_2]$ in the case of tetrahydrofurfuryl alcohol, for instance), while the higher propensity to soot of alkyl-substituted furans notably stems from the inclusion of groups promoting soot formation such as $[C-(C_f)(H)_3]$ and $[C-(C_f)(C)-(H)_2]$. The trends observed in the case of the furans substituted with oxygenated groups, moreover, illustrated that the farther the branching is from the oxygen in the furan ring, the lower the sooting tendency. Finally,

https://doi.org/10.1021/acs.energyfuels.5c00385
Energy Fuels 2025, 39, 6991−7011

the results obtained with terpenes were found to agree with the trends reported in ref 30, except in the case of myrcene (MC), which was found to be sootier than kerosene, while its YSI was found to be identical to that of geraniol in ref 30. As for the predictions of our GCM, which properly reproduces the results by ref 30 with citronellal, geranial, linalool, geraniol, 1,8-cineole, and β-ocimene, they confirm that MC should soot more than all the other tested terpenes. While strengthening the validity of the experimental observations reported in the present work, this observation still paves the way for complementary analyses aimed at better interpreting the reasons explaining the diverging trend.

- Although pyrolysis oils (POs) are the fuels exhibiting the lowest UI among the additives tested herein, their high water content and low pH and energy density still represent major challenges limiting their use as drop-in fuels without their chemical and physical properties being further upgraded.

In conclusion, the present work contributed to the identification of low-sooting fuel blends from different chemical functionalities and, in addition, also allowed extending the predictive capability of a comprehensive group contribution model. As mentioned in a reference review dealing with recent advances in the fields of the characterization of the propensity to soot of hydrocarbons for the development of sustainable fuels,[109] some avenues, however, need to be further explored. These notably include a thorough assessment of the sooting tendency of additional molecules and the development of predictive emission indices (as we previously did in ref 108). Furthermore, although group contribution models are very useful in providing insights into how the chemical structure of hydrocarbons and oxygenated molecules affect soot production, they do not allow exploring in detail the reaction mechanisms responsible for the formation and growth of polycyclic aromatic hydrocarbons and soot. Complementary kinetic modeling works would thus be of high interest to improve our understanding of the chemistry at play during the combustion of the tested additives while possibly improving the prediction of their propensity to soot. Finally, and from a more general perspective, different aspects of biofuel production, which, however, fall outside of the scope of the present study, would still need to be investigated before reaching the stage of commercialization of drop-in sustainable additives compatible with existing infrastructures and meeting current societal transportation requirements. These notably include the major challenges associated with production cost, life cycle pollutant emissions, and regulatory approvals,[110] thus supporting the need for complementary and interdisciplinary research.

AUTHOR INFORMATION

Corresponding Author

Romain Lemaire − *TFT Laboratory, Department of Mechanical Engineering, École de technologie supérieure, Montréal, Québec H3C 1K3, Canada;* orcid.org/0009-0003-5106-3925; Phone: 514 396-8727; Email: romain.lemaire@etsmtl.ca

Authors

Carl Rainville − *TFT Laboratory, Department of Mechanical Engineering, École de technologie supérieure, Montréal, Québec H3C 1K3, Canada*

Simon Laflamme − *TFT Laboratory, Department of Mechanical Engineering, École de technologie supérieure, Montréal, Québec H3C 1K3, Canada*

Ibrahima Souno − *TFT Laboratory, Department of Mechanical Engineering, École de technologie supérieure, Montréal, Québec H3C 1K3, Canada*

Patrice Seers − *TFT Laboratory, Department of Mechanical Engineering, École de technologie supérieure, Montréal, Québec H3C 1K3, Canada*

Complete contact information is available at: https://pubs.acs.org/10.1021/acs.energyfuels.5c00385

Author Contributions

Conceptualization: R.L.; methodology: R.L.; investigation and formal analysis: C.R., R.L., S.L., I.S.; funding acquisition: R.L.; project administration: R.L.; resources: R.L.; supervision: R.L., and P.S.; validation: R.L.; visualization: C.R., and R.L.; writing original draft preparation: C.R., and R.L.; writing, review, and editing: R.L.

Notes

The authors declare no competing financial interest.

ACKNOWLEDGMENTS

This research was supported by the Natural Sciences and Engineering Research Council of Canada (NSERC) and the Icam School of Engineering in France. Furthermore, the authors thank Stephane Godbout, Joahnn Palacios and Laura Daniela Mila Saavedra from the Research and Development Institute for the Agri-Environment (IRDA) in Quebec for providing the tested pyrolysis oils as well as Brice Martial Kamdem from ÉTS for his help in the emulsification tests.

REFERENCES

(1) Michelsen, H. A. Probing soot formation, chemical and physical evolution, and oxidation: A review of in situ diagnostic techniques and needs. *Proc. Combust. Inst.* **2017**, *36*, 717−735.

(2) Richter, H.; Howard, J. B. Formation of polycyclic aromatic hydrocarbons and their growth to soot—a review of chemical reaction pathways. *Prog. Energy Combust. Sci.* **2000**, *26*, 565−608.

(3) McEnally, C. S.; Pfefferle, L. D.; Atakan, N.; Kohse-Höinghaus, K. Studies of aromatic hydrocarbon formation mechanisms in flames: progress towards closing the fuel gap. *Prog. Energy Combust. Sci.* **2006**, *32*, 247−294.

(4) Wang, H. Formation of nascent soot and other condensed-phase materials in flames. *Proc. Combust. Inst.* **2011**, *33*, 41−67.

(5) Michelsen, H. A.; Colket, M. B.; Bengtsson, P.-E.; D'Anna, A.; Desgroux, P.; Haynes, B. S.; Miller, J. H.; Nathan, G. J.; Pitsch, H.; Wang, H. A review of terminology used to describe soot formation and evolution under combustion and pyrolytic conditions. *ACS Nano* **2020**, *14*, 12470−12490.

(6) Xu, L.; Wang, Y.; Liu, D. Effects of oxygenated biofuel additives on soot formation: A comprehensive review of laboratory-scale studies. *Fuel* **2022**, *313*, 122635.

(7) Lee, J.; Oh, H.; Bae, C. Combustion process of JP-8 and fossil Diesel fuel in a heavy duty diesel engine using two-color thermometry. *Fuel* **2012**, *102*, 264−273.

(8) Patil, K. R.; Thipse, S. S. Experimental investigation of CI engine combustion, performance and emissions in DEE−kerosene−diesel blends of high DEE concentration. *Energy Convers. Manage.* **2015**, *89*, 396−408.

(9) Pratap Singh, A.; Agarwal, A. K. Diesoline, Diesohol, and Diesosene Fuelled HCCI Engine Development. *J. Energy Resour. Technol.* **2016**, *138*, 052212.

(10) Chen, L.; Ding, S.; Liu, H.; Lu, Y.; Li, Y.; Roskilly, A. P. Comparative study of combustion and emissions of kerosene (RP-3),

kerosene-pentanol blends and diesel in a compression ignition engine. *Appl. Energy* **2017**, *203*, 91−100.
(11) Yang, W.; Tay, K. L.; Kong, K. W. Impact of Various Factors on the Performance and Emissions of Diesel Engine Fueled by Kerosene and Its Blend with Diesel. *Energy Procedia* **2017**, *142*, 1564−1569.
(12) Ashour, M. K.; Elwardany, A. E. Addition of two kerosene-based fuels to diesel−biodiesel fuel: Effect on combustion, performance and emissions characteristics of CI engine. *Fuel* **2020**, *269*, 117473.
(13) Bhowmik, S.; Paul, A.; Panua, R.; Ghosh, S. K. Performance, combustion and emission characteristics of a diesel engine fueled with diesel-kerosene-ethanol: A multi-objective optimization study. *Energy* **2020**, *211*, 118305.
(14) Wei, S.; Sun, L.; Wu, L.; Yu, Z.; Zhang, Z. Study of combustion characteristics of diesel, kerosene (RP-3) and kerosene-ethanol blends in a compression ignition engine. *Fuel* **2022**, *317*, 123468.
(15) Wang, Z.; Li, X.; Xiang, L.; Huang, Y.; Lang, B.; Cheng, X.; Zhang, J. Potential of kerosene-diesel blends as alternative fuels for diesel engines: Perspectives from spray combustion characteristics. *Fuel* **2023**, *335*, 127112.
(16) Khorsheed Zangana, L. M.; Yaseen, A. H.; Hassan, Q. H.; Mohammed, M. M.; Mohammed, M. F.; Alalwan, H. A. Investigated kerosene-diesel fuel performance in internal combustion engine. *Clean. Eng. Technol.* **2023**, *12*, 100591.
(17) Aydin, H. Scrutinizing the combustion, performance and emissions of safflower biodiesel−kerosene fueled diesel engine used as power source for a generator. *Energy Convers. Manage.* **2016**, *117*, 400−409.
(18) Bayındır, H.; Zerrakki Işık, M.; Aydın, H. Evaluation of combustion, performance and emission indicators of canola oil-kerosene blends in a power generator diesel engine. *Appl. Therm. Eng.* **2017**, *114*, 234−244.
(19) Roy, M. M.; Wang, W.; Alawi, M. Performance and emissions of a diesel engine fueled by biodiesel−diesel, biodiesel−diesel-additive and kerosene−biodiesel blends. *Energy Convers. Manage.* **2014**, *84*, 164−173.
(20) Ekaab, N. S.; Hamza, N. H.; Chaichan, M. T. Performance and emitted pollutants assessment of diesel engine fuelled with biokerosene. *Case Stud. Therm. Eng.* **2019**, *13*, 100381.
(21) Gad, M. S.; Ismail, M. S. Effect of waste cooking oil biodiesel blending with gasoline and kerosene on diesel engine performance, emissions and combustion characteristics. *Process Saf. Environ. Prot.* **2021**, *149*, 1−10.
(22) Ravindra; Aruna, M.; Vardhan, H. Effect of injection pressure on output of a CI engine fuelled with raw Cardanol and kerosene blends. *Mater. Today: Proc.* **2023**, *92*, 177−181.
(23) Yu, L.; Wu, H.; Zhao, W.; Qian, Y.; Zhu, L.; Lu, X. Experimental study on the application of n-butanol and n-butanol/kerosene blends as fuel for spark ignition aviation piston engine. *Fuel* **2021**, *304*, 121362.
(24) Zhang, S.; Zhao, Z.; Wang, L.; Yu, C.; Yang, Z.; Wang, S. Experimental study on the effects of injection pressure on the combustion in a SI aviation piston engine fueled with kerosene. *Fuel* **2023**, *354*, 128875.
(25) Suchocki, T.; Kazimierski, P.; Lampart, P.; Januszewicz, K.; Bialecki, T.; Gawron, B.; Janicka, A. A comparative study of pentanol (C5 alcohol) and kerosene blends in terms of gas turbine engine performance and exhaust gas emission. *Fuel* **2023**, *334*, 126741.
(26) Tay, K. L.; Yang, W.; Mohan, B.; An, H.; Zhou, D.; Yu, W. Development of a robust and compact kerosene−diesel reaction mechanism for diesel engines. *Energy Convers. Manage.* **2016**, *108*, 446−458.
(27) Tay, K. L.; Yang, W.; Mohan, B.; Zhou, D.; Yu, W.; Zhao, F. Development of a reduced kerosene−diesel reaction mechanism with embedded soot chemistry for diesel engines. *Fuel* **2016**, *181*, 926−934.
(28) E, J.; Xu, W.; Ma, Y.; Tan, D.; Peng, Q.; Tan, Y.; Chen, L. Soot formation mechanism of modern automobile engines and methods of reducing soot emissions: A review. *Fuel Process. Technol.* **2022**, *235*, 107373.
(29) Jin, Z.-H.; Chen, J.-T.; Li, W.; Song, S.-B.; Yang, J.-Z.; Tian, Z.-Y. Pyrolysis of 2-methylfuran/jet fuel surrogate blends: An experimental and kinetic modeling study. *Combust. Flame* **2021**, *232*, 111509.
(30) Zhu, J.; Alegre-Requena, J. V.; Cherry, P.; Curtis, D.; Harvey, B. G.; Jabed, M. A.; Kim, S.; McEnally, C. S.; Pfefferle, L. D.; Woodroffe, J.-D. Sooting tendencies of terpenes and hydrogenated terpenes as sustainable transportation biofuels. *Proc. Combust. Inst.* **2023**, *39*, 877−887.
(31) Dagaut, P.; Cathonnet, M. The ignition, oxidation, and combustion of kerosene: A review of experimental and kinetic modeling. *Prog. Energy Combust. Sci.* **2006**, *32*, 48−92.
(32) ASTM International. *Standard Test Method for Smoke Point of Kerosene and Aviation Turbine Fuel*, ASTM D1322-19: West Conshohocken, PA, 2019.
(33) ASTM International. *Standard Specification for Aviation Turbine Fuel Containing Synthesized Hydrocarbons*, ASTM D7566-21: West Conshohocken, PA, 2021.
(34) Eddings, E. G.; Yan, S.; Ciro, W.; Sarofim, A. F. Formulation of a surrogate for the simulation of jet fuel pool fires. *Combust. Sci. Technol.* **2005**, *177*, 715−739.
(35) Aksit, I. A.; Moss, J. B. Model fuels to reproduce the sooting behaviour of aviation kerosene. *Fuel* **2005**, *84*, 239−245.
(36) Honnet, S.; Seshadri, K.; Niemann, U.; Peters, N. A surrogate fuel for kerosene. *Proc. Combust. Inst.* **2009**, *32*, 485−492.
(37) Dooley, S.; Won, S. H.; Heyne, J.; Farouk, T. I.; et al. The experimental evaluation of a methodology for surrogate fuel formulation to emulate gas phase combustion kinetic phenomena. *Combust. Flame* **2012**, *159*, 1444−1466.
(38) Kim, D.; Martz, J.; Violi, A. A surrogate for emulating the physical and chemical properties of conventional jet fuel. *Combust. Flame* **2014**, *161*, 1489−1498.
(39) Yu, W.; Yang, W.; Tay, K.; Zhao, F. An optimization method for formulating model-based jet fuel surrogate by emulating physical, gas phase chemical properties and threshold sooting index (TSI) of real jet fuel under engine relevant conditions. *Combust. Flame* **2018**, *193*, 192−217.
(40) Rainville, C.; Lemaire, R.; Seers, P. Analysis of the sooting propensity of a jet fuel surrogate blended with different oxygenated molecules. In *Proceedings of the Combustion Institute—Canadian Section (CI/CS), Spring Technical Meeting*, 2022.
(41) Xue, X.; Hui, X.; Vannorsdall, P.; Singh, P.; Sung, C.-J. The blending effect on the sooting tendencies of alternative/conventional jet fuel blends in non-premixed flames. *Fuel* **2019**, *237*, 648−657.
(42) Kewley, J.; Jackson, S. The burning of mineral oil in wick fed lamps. *J. Inst. Pet. Technol.* **1927**, *13*, 364−397.
(43) Minchin, S. T. Luminous stationary flames: the quantitative relationship between flame dimensions at the sooting point and chemical composition, with special reference to petroleum hydrocarbons. *J. Inst. Pet. Technol.* **1931**, *17*, 102−120.
(44) Calcote, H. F.; Manos, D. M. Effect of molecular structure on incipient soot formation. *Combust. Flame* **1983**, *49*, 289−304.
(45) Olson, D. B.; Pickens, J. C.; Gill, R. J. The effects of molecular structure on soot formation II. Diffusion Flames. *Combust. Flame* **1985**, *62*, 43−60.
(46) Gill, R. J.; Olson, D. B. Estimation of soot thresholds for fuel mixtures. *Combust. Sci. Technol.* **1984**, *40*, 307−315.
(47) Barrientos, E. J.; Lapuerta, M.; Boehman, A. L. Group additivity in soot formation for the example of C-5 oxygenated hydrocarbon fuels. *Combust. Flame* **2013**, *160*, 1484−1498.
(48) McEnally, C.; Pfefferle, L. Improved sooting tendency measurements for aromatic hydrocarbons and their implications for naphthalene formation pathways. *Combust. Flame* **2007**, *148*, 210−222.
(49) Lemaire, R.; Lapalme, D.; Seers, P. Analysis of the sooting propensity of C-4 and C-5 oxygenates: comparison of sooting indexes

https://doi.org/10.1021/acs.energyfuels.5c00385
Energy Fuels 2025, 39, 6991−7011

issued from laser-based experiments and group additivity approaches. *Combust. Flame* **2015**, *162*, 3140−3155.
(50) Watson, R. J.; Botero, M. L.; Ness, C. J.; Morgan, N. M.; Kraft, M. M. An improved methodology for determining threshold sooting indices from smoke point lamps. *Fuel* **2013**, *111*, 120−130.
(51) Graziano, B.; Ottenwälder, T.; Manderfeld, D.; Pischinger, S.; Grünefeld, G. Advanced Methodology for the Detection of Smoke Point Heights in Hydrocarbon Flames. *Energy Fuels* **2018**, *32*, 3908−3919.
(52) Rubio-Gomez, G.; Corral-Gomez, L.; Soriano, J. A.; Gomez, A.; Castillo-Garcia, F. J. Vision based algorithm for automated determination of smoke point of diesel blends. *Fuel* **2019**, *235*, 595−602.
(53) Cohen, N.; Benson, S. W. Estimation of heats of formation of organic compounds by additivity methods. *Chem. Rev.* **1993**, *93*, 2419−2438.
(54) Pepiot-Desjardins, P.; Pitsch, H.; Malhotra, R.; Kirby, S.; Boehman, A. Structural group analysis for soot reduction tendency of oxygenated fuels. *Combust. Flame* **2008**, *154*, 191−205.
(55) Das, D. D.; St John, P. C.; McEnally, C. S.; Kim, S.; Pfefferle, L. D. Measuring and predicting sooting tendencies of oxygenates, alkanes, alkenes, cycloalkanes, and aromatics on a unified scale. *Combust. Flame* **2018**, *190*, 349−364.
(56) Lemaire, R.; Le Corre, G.; Nakouri, M. Predicting the propensity to soot of hydrocarbons and oxygenated molecules by means of structural group contribution factors derived from the processing of unified sooting indexes. *Fuel* **2021**, *302*, 121104.
(57) Boehm, R. C.; Yang, Z.; Heyne, J. S. Threshold Sooting Index of Sustainable Aviation Fuel Candidates from Composition Input Alone: Progress toward Uncertainty Quantification. *Energy Fuels* **2022**, *36*, 1916−1928.
(58) Jenkins, R. W.; Munro, M.; Nash, S.; Chuck, C. J. Potential renewable oxygenated biofuels for the aviation and road transport sectors. *Fuel* **2013**, *103*, 593−599.
(59) Chuck, C. J.; Donnelly, J. The compatibility of potential bioderived fuels with Jet A-1 aviation kerosene. *Appl. Energy* **2014**, *118*, 83−91.
(60) Marsh, N. D.; Preciado, I.; Eddings, E. G.; Sarofim, A. F.; Palotas, A. B.; Robertson, J. D. Evaluation of organometallic fuel additives for soot suppression. *Combust. Sci. Technol.* **2007**, *179*, 987−1001.
(61) Rojas-Michaga, M. F.; Michailos, S.; Cardozo, E.; Akram, M.; Hughes, K. J.; Ingham, D.; Pourkashanian, M. Sustainable aviation fuel (SAF) production through power-to-liquid (PtL): A combined techno-economic and life cycle assessment. *Energy Convers. Manage.* **2023**, *292*, 117427.
(62) Lahijani, P.; Mohammadi, M.; Mohamed, A. R.; Ismail, F.; Lee, K. T.; Amini, G. Upgrading biomass-derived pyrolysis bio-oil to bio-jet fuel through catalytic cracking and hydrodeoxygenation: A review of recent progress. *Energy Convers. Manage.* **2022**, *268*, 115956.
(63) Won, S. H.; Rock, N.; Lim, S. J.; Nates, S.; Carpenter, D.; Emerson, B.; Lieuwen, T.; Edwards, T.; Dryer, F. L. Preferential vaporization impacts on lean blow-out of liquid fueled combustors. *Combust. Flame* **2019**, *205*, 295−304.
(64) Xiang, Z.; Chen, K.; McEnally, C. S.; Pfefferle, L. D. Sooting tendencies of diesel fuel component mixtures follow a linear mixing rule. **2022**, ChemRxiv-2022-xrgnf.
(65) Edwards, T. Reference jet fuels for combustion testing. In *55th AIAA Aerospace Sciences Meeting*; American Institute of Aeronautics and Astronautics: Grapevine, TX, 2017.
(66) Watson, K. M.; Nelson, E. F.; Murphy, G. B. Characterization of petroleum fractions. *Ind. Eng. Chem.* **1935**, *27*, 1460−1464.
(67) Plazas Tovar, L.; Wolf Maciel, M. R.; Maciel Filho, R.; Batistella, C. B.; Celis Ariza, O. J.; Medina, L. Overview and Computational Approach for Studying the Physicochemical Characterization of High-Boiling-Point Petroleum Fractions (350°C$^+$). *Oil Gas Sci. Technol.* **2012**, *67*, 451−477.
(68) Boehm, R. C.; Coburn, A. A.; Yang, Z.; Wanstall, C. T.; Heyne, J. S. Blend Prediction Model for the Freeze Point of Jet Fuel Range Hydrocarbons. *Energy Fuels* **2022**, *36*, 12046−12053.
(69) ASTM International. *Standard Test Method for Estimation of Net Heat of Combustion of Aviation Fuels*, ASTM D3338/D3338M-20a: West Conshohocken, PA, 2020.
(70) *NIST Chemistry WebBook, NIST Standard Reference Database Number 69*; Linstrom, P. J., Mallard, W. G., Eds.; National Institute of Standards and Technology: Gaithersburg MD, 20899, 2024.
(71) Fischer, O.; Lemaire, R.; Bensakhria, A. Thermogravimetric analysis and kinetic modeling of the pyrolysis of different biomass types by means of model-fitting, model-free and network modeling approaches. *J. Therm. Anal. Calorim.* **2024**, *149*, 10941−10963.
(72) Brassard, P.; Godbout, S.; Raghavan, V.; Palacios, J. H.; Grenier, M.; Zegan, D. The production of engineered biochars in a vertical auger pyrolysis reactor for carbon sequestration. *Energies* **2017**, *10*, 288.
(73) Álvarez-Chávez, B. J.; Godbout, S.; Le Roux, E.; Palacios, J. H.; Raghavan, V. Bio-oil yield and quality enhancement through fast pyrolysis and fractional condensation concepts. *Biofuel Res. J.* **2019**, *24*, 1054−1064.
(74) Imam, T.; Capareda, S. Characterization of bio-oil, syn-gas and bio-char from switchgrass pyrolysis at various temperatures. *J. Anal. Appl. Pyrolysis* **2012**, *93*, 170−177.
(75) Chandrasekaran, S. R.; Murali, D.; Marley, K. A.; Larson, R. A.; Doll, K. M.; Moser, B. R.; Scott, J.; Sharma, B. K. Antioxidants from Slow Pyrolysis Bio-Oil of Birch Wood: Application for Biodiesel and Biobased Lubricants. *ACS Sustain. Chem. Eng.* **2016**, *4*, 1414−1421.
(76) Ben, H.; Wu, F.; Wu, Z.; Han, G.; Jiang, W.; Ragauskas, A. J. A Comprehensive Characterization of Pyrolysis Oil from Softwood Barks. *Polymers* **2019**, *11*, 1387.
(77) Elehinafe, F. B.; Adisa, H. A.; Adesina, A.; Okedere, O. B.; Unen, U. E. Economic potentials of pyro bio-oil production from sawdust generated by southwest, Nigeria - A simulation-based approach. *Case Stud. Chem. Environ. Eng.* **2024**, *9*, 100590.
(78) Ren, S.; Ye, X. P.; Borole, A. P.; Kim, P.; Labbé, N. Analysis of switchgrass-derived bio-oil and associated aqueous phase generated in a semi-pilot scale auger pyrolyzer. *J. Anal. Appl. Pyrolysis* **2016**, *119*, 97−103.
(79) Mateus, M. M.; Bordado, J. M.; Galhano dos Santos, R. Estimation of higher heating value (HHV) of bio-oils from thermochemical liquefaction by linear correlation. *Fuel* **2021**, *302*, 121149.
(80) Lin, B.-J.; Chen, W.-H.; Budzianowski, W. M.; Hsieh, C.-T.; Lin, P.-H. Emulsification analysis of bio-oil and diesel under various combinations of emulsifiers. *Appl. Energy* **2016**, *178*, 746−757.
(81) De Luna, M. D. G.; Cruz, L. A. D.; Chen, W.-H.; Lin, B.-J.; Hsieh, T.-H. Improving the stability of diesel emulsions with high pyrolysis bio-oil content by alcohol co-surfactants and high shear mixing strategies. *Energy* **2017**, *141*, 1416−1428.
(82) Liu, K.; Zhao, W.; Guo, T.; Lei, Q.; Guan, Y.; Wang, D.; Cui, M.; Fu, S.; Zhao, J.; Zong, Z.; Wei, X. Emulsification and Performance Measurement of Bio-oil with Diesel. *Waste Biomass Valorization* **2021**, *12*, 2933−2944.
(83) Benson, S. W.; Buss, J. H. Additivity rules for the estimation of molecular properties. Thermodynamic properties. *J. Chem. Phys.* **1958**, *29*, 546−572.
(84) Cohen, N.; Benson, S. W. Estimation of heats of formation of organic compounds by additivity methods. *Chem. Rev.* **1993**, *93*, 2419−2438.
(85) Somers, K. P. On the pyrolysis and combustion of furans: quantum chemical, statistical rate theory, and chemical kinetic modelling studies, Ph.D. Thesis; National University of Ireland: Galway, 2014.
(86) Lemaire, R.; Menanteau, S. Modeling laser-induced incandescence of Diesel soot-Implementation of an advanced parameterization procedure applied to a refined LII model accounting for shielding effect and multiple scattering within aggregates for α_T and E(m) assessment. *Appl. Phys. B:Lasers Opt.* **2021**, *127*, 138.

https://doi.org/10.1021/acs.energyfuels.5c00385
Energy Fuels 2025, 39, 6991−7011

(87) Lemaire, R.; Menanteau, S. Study of the wavelength dependence of the absorption function of diesel soot by LII modeling integrating the effect of multiple scattering within aggregates. *Appl. Phys. B:Lasers Opt.* **2023**, *129*, 79.
(88) Lemaire, R.; Wang, W.; Menanteau, S. Kinetic Modeling of the Devolatilization of Pulverized Coal, Poplar Wood, and Their Blends in a Thermogravimetric Analyzer and a Flat Flame Reactor. *ACS Omega* **2023**, *8*, 29455−29467.
(89) Billerot, P. L.; Fleischmann, A.; Tétrault, P.; Lemaire, R.; Seers, P. *Non-Evaporating Fuel Spray Tip Penetration: A Comparison between Phenomenological Models and Experiments*, SAE Technical Paper 2023-01-1635, 2023.
(90) Yang, Y.; Boehman, A. L.; Santoro, R. J. A study of jet fuel sooting tendency using the threshold sooting index (TSI) model. *Combust. Flame* **2007**, *149*, 191−205.
(91) Zhang, C.; Hui, X.; Lin, Y.; Sung, C.-J. Recent development in studies of alternative jet fuel combustion: Progress, challenges, and opportunities. *Renewable Sustainable Energy Rev.* **2016**, *54*, 120−138.
(92) Lemaire, R.; Therssen, E.; Pauwels, J. F.; Desgroux, P. Experimental comparison of soot formation in turbulent flames of kerosene and surrogate model fuels. In *Combustion-generated Fine Carbonaceous Particles*; Bockhorn, H., D'Anna, A., Sarofim, A. F., Wang, H., Eds.; KIT Scientific Publishing: Karlsruhe, 2019; pp 619−636.
(93) Saraee, H. S.; Hughes, K. J.; Pourkashanian, M. A compact chemical kinetic mechanism for modelling isocetane. *J. Energy Inst.* **2023**, *108*, 101253.
(94) McEnally, C. S.; Pfefferle, L. D. Sooting Tendencies of Oxygenated Hydrocarbons in Laboratory-Scale Flames. *Environ. Sci. Technol.* **2011**, *45*, 2498−2503.
(95) Al Shebli, M. N.; Raj, A.; Elkadi, M.; Anjum, D.; Pena, G. D. J.; Prabhu, A. Fuel oxygenation as a novel method to reduce sooting propensity of fuels: An investigation with gasoline surrogate fuels. *Fuel* **2022**, *324*, 124562.
(96) Zhu, J. Sooting Tendencies and Soot Formation Pathways of Alternative Fuels and Compounds, Ph.D. Dissertation, Yale University, New Haven. 2023. Retrieved from https://www.proquest.com/dissertations-theses/sooting-tendencies-soot-formation-pathways/docview/2781505536/se-2.
(97) Sudholt, A.; Cai, L.; Heyne, J.; Haas, F. M.; Pitsch, H.; Dryer, F. L. Ignition characteristics of a bio-derived class of saturated and unsaturated furans for engine applications. *Proc. Combust. Inst.* **2015**, *35*, 2957−2965.
(98) Wang, C.; Xu, H.; Daniel, R.; Ghafourian, A.; Herreros, J. M.; Shuai, S.; Ma, X. Combustion characteristics and emissions of 2-methylfuran compared to 2,5-dimethylfuran, gasoline and ethanol in a DISI engine. *Fuel* **2013**, *103*, 200−211.
(99) Tran, L.-S.; Verdicchio, M.; Monge, F.; Martin, R. C.; Bounaceeur, R.; Sirjean, B.; Glaude, P.-A.; Alzueta, M. U.; Battin-Leclerc, F. An experimental and modeling study of the combustion of tetrahydrofuran. *Combust. Flame* **2015**, *162*, 1899−1918.
(100) Pahima, E.; Hoz, S.; Ben-Tzion, M.; Major, D. T. Computational design of biofuels from terpenes and terpenoids. *Sustain. Energy Fuels* **2019**, *3*, 457−466.
(101) Oasmaa, A.; Czernik, S. Fuel oil quality of biomass pyrolysis oils-state of the art for the end users. *Energy Fuels* **1999**, *13*, 914−921.
(102) Kadota, T.; Yamasaki, H. Recent advances in the combustion of water fuel emulsion. *Prog. Energy Combust. Sci.* **2002**, *28*, 385−404.
(103) Greenhalf, C. E.; Nowakowski, D. J.; Harms, A. B.; Titiloye, J. O.; Bridgwater, A. V. A comparative study of straw. Perennial grasses and hardwoods in terms of fast pyrolysis products. *Fuel* **2013**, *108*, 216−230.
(104) Qiu, B.; Tao, X.; Wang, J.; Liu, Y.; Li, S.; Chu, H. Research progress in the preparation of high-quality liquid fuels and chemicals by catalytic pyrolysis of biomass: A review. *Energy Convers. Manage.* **2022**, *261*, 115647.
(105) Kabir, G.; Hameed, B. H. Recent progress on catalytic pyrolysis of lignocellulosic biomass to high-grade bio-oil and bio-chemicals. *Renewable Sustainable Energy Rev.* **2017**, *70*, 945−967.
(106) Chen, X.; Che, Q.; Li, S.; Liu, Z.; Yang, H.; Chen, Y.; Wang, X.; Shao, J.; Chen, H. Recent developments in lignocellulosic biomass catalytic fast pyrolysis: Strategies for the optimization of bio-oil quality and yield. *Fuel Process. Technol.* **2019**, *196*, 106180.
(107) Wang, W.; Lemaire, R.; Bensakhria, A.; Luart, D. Review on the catalytic effects of alkali and alkaline earth metals (AAEMs) including sodium, potassium, calcium and magnesium on the pyrolysis of lignocellulosic biomass and on the co-pyrolysis of coal with biomass. *J. Anal. Appl. Pyrolysis* **2022**, *163*, 105479.
(108) Lemaire, R.; Boudreau, A.; Seers, P. Performance and emissions of a DISI engine fueled with gasoline/ethanol and gasoline/C-4 oxygenate blends − Development of a PM index correlation for particulate matter emission assessment. *Fuel* **2019**, *241*, 1172−1183.
(109) Pfefferle, L. D.; Kim, S.; Kumar, S.; McEnally, C. S.; Pérez-Soto, R.; Xiang, Z.; Xuan, Y. Sooting tendencies: Combustion science for designing sustainable fuels with improved properties. *Proc. Combust. Inst.* **2024**, *40*, 105750.
(110) Bergthorson, J. B.; Thomson, M. J. A review of the combustion and emissions properties of advanced transportation biofuels and their impact on existing and future engines. *Renewable Sustainable Energy Rev.* **2015**, *42*, 1393−1417.

https://doi.org/10.1021/acs.energyfuels.5c00385
Energy Fuels 2025, 39, 6991−7011